Spectrally indistinguishable biphotons via dual processes of spontaneous four-wave mixing

Hui-Min Zhao,[1,2] M. Artoni,[3,4,*] G. C. La Rocca,[5,†] and Jin-Hui Wu[2,‡]

[1]*College of Physics and Hebei Key Laboratory of Photophysics Research and Application, Hebei Normal University, Shijiazhuang, Hebei 050024, China*
[2]*School of Physics and Center for Quantum Sciences, Northeast Normal University, Changchun 130024, China*
[3]*Department of Chemistry and Physics of Materials, University of Brescia, Italy*
[4]*European Laboratory for Non-Linear Spectroscopy, Sesto Fiorentino, Italy*
[5]*NEST, Scuola Normale Superiore, Piazza dei Cavalieri 7, I-56126 Pisa, Italy*

(Dated: November 26, 2025)

We model the generation of multiple photon pairs (*biphotons*) through engineering of coexisting nearly resonant two spontaneous four-wave-mixing (SFWM) processes in five-level atoms driven to a quasi-dark state trapping regime. This is achieved through a suitable choice of two pump and one coupling beams whose spectral profiles are taken into account *both* to provide realistic estimates for the effects of their linewidths on atomic populations, coherences and photon correlations *and* to engineer the joint spectral amplitude (JSA) distributions of generated biphotons directly by tuning the beams' parameters. We specifically leverage this tunability to control the degree of spectral indistinguishability of two biphotons with ultra-narrow linewidths. The large degree of indistinguishability achievable in our model can be harnessed for advanced applications in quantum communication and information processing and potentially adapted to compatible solid-state interfaces.

I. INTRODUCTION

Entangled photon pairs (biphotons) are a cornerstone of optical quantum technologies [1–6], with applications spanning quantum key distribution [7, 8], quantum cryptography [9], quantum computing [10, 11], and quantum teleportation [12, 13]. In these applications, photon indistinguishability – ensuring that photons are identical in frequency, polarization, spatial mode, and temporal characteristics – is crucial for achieving high-fidelity entangled states and robust quantum interference [14–19]. Indistinguishable photons minimize cross-talk and enhance interference visibility, both essential for secure communication and accurate information processing.

Various nonlinear optical processes, including spontaneous parametric down-conversion (SPDC) [20–23] and spontaneous four-wave-mixing (SFWM) [24–33], have been employed to generate entangled photon pairs. The former converts a photon from a strong (laser) pump into a pair of signal and idler photons by a second-order ($\chi^{(2)}$) nonlinear optical process that is only present in non-centrosymmetric crystals. The latter converts two photons from one or two strong laser pump(s) into two single photons by a third-order ($\chi^{(3)}$) nonlinear optical process. Conversely, SFWM processes are present in a vast array of materials *viz.* laser-cooled, room-temperature or hot atoms, integrated photonic chips and optical fibers. Furthermore, biphotons generated in nonlinear crystals via SPDC have such large bandwidths (THz) that they do not match the working bandwidths of quantum memories or frequency conversion devices that are to be interfaced. Cavity-enhanced methods to reduce the linewidths of SPDC biphotons can still be used though they are far more cumbersome than directly generating SFWM biphotons with intrinsically narrow bandwidths [34–37]. Additionally, operating SFWM processes near an atomic resonance can enable high generation rates of biphotons even at low optical powers [33, 38]. Resonant enhancement of SPDC processes is also possible but often more challenging to implement in the $\chi^{(2)}$ materials.

SFWM processes in atoms are especially amenable to achieving the control of spectral properties of photon pairs owing to the native (spectral) tunability of the underlying $\chi^{(3)}$ optical response. By tailoring its dispersion, photon pairs can be generated in an atomic sample with a spread of different target frequencies. Such a remarkable flexibility is important for applications involving quantum states that rely on spectrally tunable biphotons [39–43]. Efficient spectral tailoring of a biphoton is especially important when multiple SFWM processes coexist in a common medium. In this case, achieving spectral overlap among *multiple biphotons* being generated is primarily challenging, as we anticipate in the present work. Spectral control of a biphoton becomes critically important when strong (photon) indistinguishability is required in, *e.g.* heralding indistinguishable single photons, whereby the detection of a photon of the pair signals the presence of its twin, or in creating single-photon superposition states that exhibit frequency entanglement [44–46].

The present work focuses on an atom-based mechanism whereby two photon pairs with ultra-narrow linewidths and a large degree of spectral indistinguishability can be efficiently created by establishing a quasi-dark state trapping regime. More specifically, this hinges on the

*Electronic address: maurizio.artoni@unibs.it
†Electronic address: giuseppe.larocca@sns.it
‡Electronic address: jhwu@nenu.edu.cn

creation of two pairs of Stokes and anti-Stokes photons, $\{\omega_{s1},\omega_{as1}\}$ and $\{\omega_{s2},\omega_{as2}\}$, via two partially overlapping SFWM processes (A and B) within the five-level atomic configuration shown by Fig. 1. Our independent biphotons can be employed to create heralded indistinguishable single-photons, *e.g.* through coincidence counting of two anti-Stokes photons from different transitions $|4\rangle \leftrightarrow |1\rangle$ and $|4\rangle \leftrightarrow |3\rangle$. Indistinguishable single photons are certainly sought for in applications such as two-photon interference and entanglement swapping [47]. Such a swapping is essential to long-distance quantum communication [48, 49]. Our independent biphotons can also be employed to create heralded single-photon superposition state involving two anti-Stokes photons [41] triggered, *e.g.* by detecting indistinguishable Stokes photons from the same $|5\rangle \leftrightarrow |2\rangle$ transition. The resulting state exhibits frequency-entanglement characteristics, akin to the well-established phenomena of path-entanglement and time-bin entanglement, that have long been fundamental to quantum information protocols [50–53]. More generally, multi-pairs generation in a single system is interesting in itself as it enhances scalability and information carrying capacity of quantum devices. A scheme to multiplex two coexisting SFWM processes in a single cold atomic setup has been used to generate a narrow-band four-photon Greenberger-Horne-Zeilinger state [54].

Moreover, it is important to recall that within this context light-atom interactions depend on the frequency distributions of driving beams involved, though the complexity of each SFWM process often makes the effects of laser linewidths being overlooked. Building upon a previously developed model [38], extended here to a five-level atomic configuration supporting two SFWM processes, we additionally incorporate the explicit linewidth effects for two pump and one coupling beams. That is, we solve density-matrix equations through energy-conserving integrations over Lorentzian spectral profiles [55–57] to evaluate the actual influences of finite laser linewidths of the beams on the spectral indistinguishability of two photon pairs. Unlike the familiar anti-diagonal spectral dispersion lines observed for monochromatic setups [34–37, 58–64], our numerical analysis confirms that finite laser linewidths give rise, as expected, to spindle-shaped distributions of two joint spectral amplitudes (JSAs) for the two $\{\omega_{s1},\omega_{as1}\}$ and $\{\omega_{s2},\omega_{as2}\}$ pairs of photons. Interestingly, we find that by primarily tuning the central frequencies of the multi-mode pump beams, both JSAs can be actively tuned to achieve nearly perfect overlap and hence a large degree of spectral indistinguishability.

II. THEORETICAL MODEL

We consider in Fig. 1 a five-level atomic system where two pump and one coupling fields of amplitudes (frequencies) E_{p1}, E_{p2}, and E_c (ω_{p1}, ω_{p2}, and ω_c) are applied upon three dipole-allowed transitions $|1\rangle \leftrightarrow |5\rangle$, $|3\rangle \leftrightarrow |5\rangle$, and $|2\rangle \leftrightarrow |4\rangle$ with dipole moments (frequencies) d_{15}, d_{35},

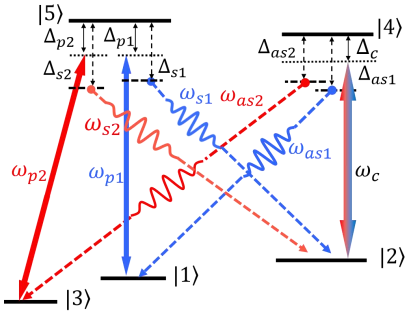

FIG. 1: Diagram of a five-level atomic system, where a pump ω_{p1} (ω_{p2}) and a coupling ω_c field are applied to generate a Stokes ω_{s1} (ω_{s2}) and an anti-Stokes ω_{as1} (ω_{as2}) photon through the SFWM process A (B) starting from ground state $|1\rangle$ ($|3\rangle$) as denoted by the blue (red) lines. In the absence of all generated fields, this five-level system reduces to two subsystems: a Λ subsystem driven by two pump fields and a two-level subsystem driven by the coupling field. A quasi-dark state trapping most populations in ground states $|1\rangle$ and $|3\rangle$ can be attained in the Λ subsystem, which enables the SFWM generation of $\{\omega_{s1},\omega_{as1}\}$ and $\{\omega_{s2},\omega_{as2}\}$ photon pairs even at exact resonance. The D_1 line of ^{87}Rb atoms is chosen here with states $|1\rangle = |5S_{1/2}, F = 1, m = -1\rangle$, $|2\rangle = |5S_{1/2}, F = 2, m = 1\rangle$, $|3\rangle = |5S_{1/2}, F = 1, m = 1\rangle$, $|4\rangle = |5P_{1/2}, F = 1, m = 0\rangle$, and $|5\rangle = |5P_{1/2}, F = 2, m = 0\rangle$ as an example.

and d_{24} (ω_{51}, ω_{53}, and ω_{42}), respectively [38]. Then, we can define the corresponding detunings $\Delta_{p1} = \omega_{51} - \omega_{p1}$, $\Delta_{p2} = \omega_{53} - \omega_{p2}$, and $\Delta_c = \omega_{42} - \omega_c$ as well as Rabi frequencies $\Omega_{p1} = E_{p1}d_{15}/2\hbar$, $\Omega_{p2} = E_{p2}d_{35}/2\hbar$, and $\Omega_c = E_c d_{24}/2\hbar$. Considering the general case of $\Delta_{p1} \neq \Delta_{p2}$, a pair of Stokes and anti-Stokes photons with Rabi frequencies $\Omega_{s1} = E_{s1}d_{25}/2\hbar$ and $\Omega_{as1} = E_{as1}d_{14}/2\hbar$ as well as detunings $\Delta_{s1} = \omega_{52} - \omega_{s1}$ and $\Delta_{as1} = \omega_{41} - \omega_{as1}$ will be generated through the SFWM process $|1\rangle \rightarrow |5\rangle \rightarrow |2\rangle \rightarrow |4\rangle \rightarrow |1\rangle$ (process A, corresponding to the blue paths in Fig. 1). Another pair of Stokes and anti-Stokes photons with Rabi frequencies $\Omega_{s2} = E_{s2}d_{25}/2\hbar$ and $\Omega_{as2} = E_{as2}d_{34}/2\hbar$ as well as detunings $\Delta_{s2} = \omega_{52} - \omega_{s2}$ and $\Delta_{as2} = \omega_{43} - \omega_{as2}$ will be generated through the other SFWM process $|3\rangle \rightarrow |5\rangle \rightarrow |2\rangle \rightarrow |4\rangle \rightarrow |3\rangle$ (process B, corresponding to the red paths in Fig. 1). It is easy to see that processes A and B share the same coupling transition but involve different pump transitions starting from ground states $|1\rangle$ and $|3\rangle$, respectively.

The population in excited state $|4\rangle$ will decay to ground states $|1\rangle$, $|2\rangle$, and $|3\rangle$ with *spontaneous emission* rates Γ_{41}, Γ_{42}, and Γ_{43} while that in state $|5\rangle$ will decay with rates Γ_{51}, Γ_{52}, and Γ_{53} to states $|1\rangle$, $|2\rangle$, and $|3\rangle$. The coherence associated with transition $|i\rangle \leftrightarrow |j\rangle$ will decay instead with *dephasing* rate given by $\gamma_{ij} = \sum_l(\Gamma_{il}+\Gamma_{jl})/2$, where $l \neq i \neq j$ may also include states that are external to our five-level atomic system. In this regard, we have indeed $\gamma_{41,42,43} = \gamma_{51,52,53} = \gamma$ with γ referring to the common natural linewidth of all six single-photon transitions. Note also that, in previous SFWM studies, coherent atom-field interactions have commonly been treated

employing *single-frequency* continuous-wave laser beams for simplicity [24, 33, 65–67]. However, laser beams always have finite linewidths, which is a feature we wish to incorporate for obtaining more accurate descriptions. That is, the pump and coupling fields should be characterized by a *spectral distribution* of frequencies ω_j, modeled here using a normalized Lorentzian profile,

$$f_j(\omega_j) = \frac{1}{\pi}\frac{\gamma_j}{(\omega_j - \varpi_j)^2 + \gamma_j^2}, \tag{1}$$

where ϖ_j and γ_j with $j \in \{p1, p2, c\}$ denote the distribution's central frequency and its half linewidth.

The basic procedure for including laser linewidths in a simpler three-level Λ system via the quantum-Langevin approach is given in Appendix A. Following the same spirit, it is viable to examine the coexisting SFWM processes A and B in our five-level atomic system with laser linewidths of all three driving fields suitably accounted for as detailed below. To reduce the complexity arising from multiple atomic levels and finite laser linewidths, we now consider that the generated Stokes and anti-Stokes fields are weak enough to be taken as perturbations. In this case, atomic populations and coherences can be decomposed into zeroth-order and first-order components with higher-order ones being safely neglected. Accordingly, we have written down Heisenberg-Langevin equations for the zeroth-order components in Appendix B and the first-order components in Appendix C for process A while in Appendix D for process B. Zeroth-order solutions reveal populations in five atomic states and coherences for the applied pump and coupling fields, while first-order solutions describe linear and nonlinear optical responses to the generated Stokes and anti-Stokes fields.

III. ATOMIC POPULATIONS

In the absence of spontaneously generated Stokes and anti-Stokes fields ($\Omega_{s1,as1,s2,as2} \to 0$), our five-level atomic system reduces to two separate subsystems: a three-level ($\{|1\rangle, |3\rangle, |5\rangle\}$) Λ-type subsystem and a two-level ($\{|2\rangle, |4\rangle\}$) subsystem. The corresponding zeroth-order dynamics involves equations for 25 density matrix elements $\rho_{ij}^{(0)}$ with $i, j \in \{1, 2, 3, 4, 5\}$, whose solutions yield both populations ($i = j$) and coherences ($i \neq j$) (see Appendix B). In particular, steady-state solutions corresponding to $\partial_t \rho_{ij}^{(0)} = 0$ can be found and used to compute the following ones averaged by all Lorentzian profiles

$$\begin{aligned}\sigma_{ij}^{(0)}(\mathcal{P}_d) &= \int_{-\infty}^{\infty} d\omega_{p1} f(\omega_{p1}) \int_{-\infty}^{\infty} d\omega_{p2} f(\omega_{p2}) \int_{-\infty}^{\infty} d\omega_c f(\omega_c) \rho_{ij}^{(0)}(\omega_{p1}, \omega_{p2}, \omega_c) \\ &= \frac{1}{\pi^3} \int_{-\infty}^{\infty}\int_{-\infty}^{\infty}\int_{-\infty}^{\infty} d\omega_{p1} d\omega_{p2} d\omega_c \frac{\gamma_{p1}\gamma_{p2}\gamma_c \rho_{ij}^{(0)}(\omega_{p1}, \omega_{p2}, \omega_c)}{[(\omega_{p1} - \varpi_{p1})^2 + \gamma_{p1}^2][(\omega_{p2} - \varpi_{p2})^2 + \gamma_{p2}^2][(\omega_c - \varpi_c)^2 + \gamma_c^2]},\end{aligned} \tag{2}$$

with $\mathcal{P}_d \equiv \{\varpi_{p1}, \varpi_{p2}, \varpi_c, \gamma_{p1}, \gamma_{p2}, \gamma_c\}$ denoting the set of driving parameters accounting for spectral distributions. They will be used to describe how the two subsystems respond together to an additional (weak) Stokes or anti-Stokes field, when atoms are driven by multi-mode pump and coupling fields. Hence, the optical responses of our five-level atomic system are in general modified or *dressed* by broadband electromagnetic excitations via $\mathcal{P}_d$.

Notice that Eq. (2) is valid only when the two pump fields are correlated in their phase fluctuations (see Appendix A). It is also well known that, under two-photon resonance conditions ($\Delta_{p1} = \Delta_{p2}$), the Λ-type subsystem exhibits the following dark state [38, 68–72]

$$|D\rangle = \frac{\Omega_{p2}}{\sqrt{\Omega_{p1}^2 + \Omega_{p2}^2}}|1\rangle - \frac{\Omega_{p1}}{\sqrt{\Omega_{p1}^2 + \Omega_{p2}^2}}|3\rangle, \tag{3}$$

so that when both $\gamma_{31} \to 0$ (*i.e.*, no ground state dephasing) and $\gamma_{p1} = \gamma_{p2} \to 0$ (*i.e.*, zero pump linewidths), most population will be trapped in $|D\rangle$ with $\sigma_{11}^{(0)} + \sigma_{33}^{(0)} \to 1$. This is critical for attaining efficient SFWM resonant biphoton generation in the presence of little linear absorption and Raman gain [33, 38]. Conversely, when the two pumps are not two-photon resonant and we account for the finite pump linewidths, our five-level atomic system will not support the ideal dark state $|D\rangle$. Deviations may be assessed by examining how two population sums $\sigma_{11}^{(0)} + \sigma_{33}^{(0)}$ and $\sigma_{22}^{(0)} + \sigma_{44}^{(0)} + \sigma_{55}^{(0)}$ vary with central pump detunings $\Delta_{p10} = \omega_{51} - \varpi_{p1}$, $\Delta_{p20} = \omega_{53} - \varpi_{p2}$ while taking a resonant coupling ($\Delta_{c0} = \omega_{42} - \varpi_c = 0$). This has been done in Fig. 2 for $\gamma_{p1} = \gamma_{p2} = \gamma_c = \gamma_L$, which shows that a narrower linewidth ($2\pi \times 20$ kHz) allows for a tighter population trapping within dark state $|D\rangle$, as $\sigma_{11}^{(0)} + \sigma_{33}^{(0)}$ remains close to unity (0.96) while $\sigma_{22}^{(0)} + \sigma_{44}^{(0)} + \sigma_{55}^{(0)}$ still being quite small around $\Delta_{p10} = \Delta_{p20}$. In contrast, a broader linewidth ($2\pi \times 200$ kHz) leads to an essential population transfer outside of dark state $|D\rangle$, as indicated by the significant decrease of $\sigma_{11}^{(0)} + \sigma_{33}^{(0)}$ in a wider range around $\Delta_{p10} = \Delta_{p20}$. That is, the common linewidth and central detunings of driving beams are both crucial for maintaining dark-state condition and hence optimizing biphoton generation. In general, dark-state trapping benefits from using a narrower common linewidth and

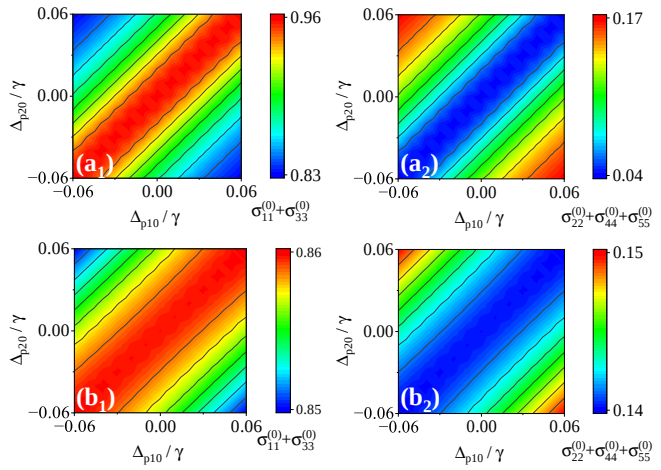

FIG. 2: Population sums $\sigma_{11}^{(0)}+\sigma_{33}^{(0)}$ (a_1,b_1) and $\sigma_{22}^{(0)}+\sigma_{44}^{(0)}+\sigma_{55}^{(0)}$ (a_2,b_2) within and outside of the dark state, respectively, plotted against central pump detunings Δ_{p10} and Δ_{p20} for a common laser linewidth $\gamma_L = \gamma_{p1,p2,c} = 2\pi \times 20$ kHz (a_1,a_2) or $2\pi \times 200$ kHz (b_1,b_2). Other parameters are $\gamma = \gamma_{54}/2 = \gamma_{53,52,51} = \gamma_{43,42,41} = 2\Gamma_{52,42} = 6\Gamma_{53,51,43,41} = 2\pi \times 3$ MHz, $\gamma_{32,31,21} = 2\pi \times 3$ kHz, $\Omega_{p1,p2} = \gamma/6$, $\Omega_c = 4\gamma$, and $\Delta_{c0} = 0$.

nearly equal central detunings of the two pumps.

IV. LINEAR AND NONLINEAR SUSCEPTIBILITIES

The Stokes and anti-Stokes photon pairs $\{\omega_{s1}, \omega_{as1}\}$ and $\{\omega_{s2}, \omega_{as2}\}$ can be generated through SFWM processes A and B as shown by blue and red paths, respectively, in Fig. 1, which involve the annihilation of different pump photons ω_{p1} and ω_{p2} while a common coupling photon ω_c. In our specific context, biphoton generation takes place through a five-level open interaction loop in a regime of quasi-dark state trapping. This is a condition that prevents population redistribution among different states and effectively makes our five-level atomic system to exhibit two nearly independent SFWM processes. This is thoroughly discussed in Appendices C and D, where we explicitly provide the full set of density-matrix equations for processes A and B, respectively.

Since the generated Stokes and anti-Stokes fields are very *weak*, the *first-order* perturbative approach with respect to Ω_{s1} and Ω_{as1} in process A while to Ω_{s2} and Ω_{as2} in process B will be employed to describe the biphoton generation mechanism. For process A, density-matrix equations can be solved in the steady state with $\partial_t \rho_{ij}^{(1)} = 0$ to obtain $\rho_{ij}^{(1)}$ containing only first-order terms of Ω_{s1} and Ω_{as1}. Note in particular that $\rho_{52}^{(1)}$ and $\rho_{41}^{(1)}$ determine polarizations $P_{52} = N_0 d_{25} \rho_{52}^{(1)}$ at the Stokes frequency and $P_{41} = N_0 d_{14} \rho_{41}^{(1)}$ at the anti-Stokes frequency, respectively, for an atomic sample of density N_0 through

$$P_{52} = \epsilon_0 \chi_{s1}^{(1)} E_{s1} + \epsilon_0 \chi_{s1,as1}^{(3)} E_{p1} E_c E_{as1}^*, \tag{4a}$$

$$P_{41} = \epsilon_0 \chi_{as1}^{(1)} E_{as1} + \epsilon_0 \chi_{as1,s1}^{(3)} E_{p1} E_c E_{s1}^*. \tag{4b}$$

Here, $\chi_{\alpha}^{(1)}$ denotes a linear susceptibility whose real and imaginary parts govern, respectively, the dispersion and absorption or (Raman gain) of ω_α photons, while $\chi_{\alpha,\beta}^{(3)}$ is a nonlinear susceptibility accounting for the subsequent generation of ω_α photons with already existing ω_β photons [33]. It is easy to learn by comparing P_{52} and P_{41} in Eq. (4) that only $\chi_{as1,s1}^{(3)}$ needs to be considered in the following discussions, while $\chi_{s1,as1}^{(3)}$ can be neglected because population $\rho_{22}^{(0)}$ in state $|2\rangle$ is vanishing so that ω_{s1} photons must be generated before ω_{as1} photons.

Before concluding this section, we briefly recall relevant optical responses of our atomic sample to the generated ω_{s1} and ω_{as1} fields in the monochromatic limit by computing in Fig. 3 susceptibilities $\chi_{s1}^{(1)}$, $\chi_{as1}^{(1)}$, and $\chi_{as1,s1}^{(3)}$ for a vanishing laser linewidth ($\gamma_L = 0$). Linear susceptibility $\chi_{s1}^{(1)}$ describes a transition channel between two weakly populated states $|5\rangle$ and $|2\rangle$ with negligible Raman gain for all values of Stokes detuning Δ_{s1}. In the anti-Stokes channel, linear susceptibility $\chi_{as1}^{(1)}$ exhibits an EIT window centered at $\Delta_{as1} = 0$ with absorption strongly suppressed between two peaks centered at $\Delta_{as1} = \pm 4\gamma$. Nonlinear susceptibility $\chi_{as1,s1}^{(1)}$ seems more prominent around both absorption peaks but is also essential around the EIT window, where we have more efficient biphoton generation as shown in the next section. With finite linewidths ($\gamma_L \neq 0$), $\chi_{as1}^{(1)}$ remains nearly unchanged, while both $\chi_{s1}^{(1)}$ and $\chi_{as1,s1}^{(3)}$ will increase noticeably. For instance, the magnitude of $\chi_{as1,s1}^{(3)}$ will increase by about 8 times at $\gamma_L = 2\pi \times 20$ kHz and about 30 times at $\gamma_L = 2\pi \times 200$ kHz, compared to that attained in the monochromatic limit (examined but not shown).

V. NONLINEAR PHOTON PAIRS GENERATION

The nonlinear spontaneous generation of Stokes and anti-Stokes photon pairs for SFWM process A can be described by the effective Hamiltonian [38]

$$\hat{H}_I(t) = \frac{\epsilon_o A}{4} \int_0^L dz \chi_{as1,s1}^{(3)} E_c(z,t) E_{p1}(z,t) \hat{E}_{s1}^-(z,t) \hat{E}_{as1}^-(z,t) + h.c., \tag{5}$$

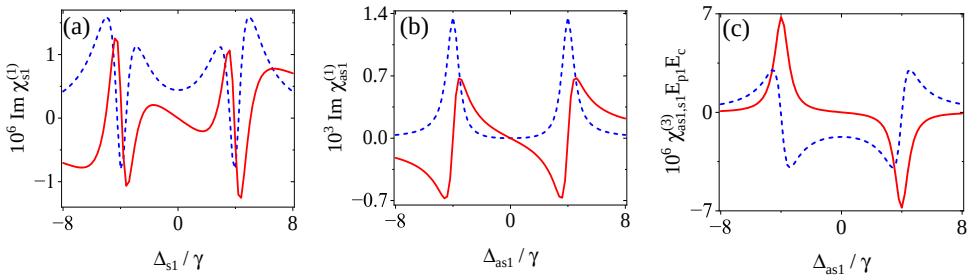

FIG. 3: Real (red-solid) and imaginary (blue-dashed) parts of (a) $\chi^{(1)}_{s1}$, (b) $\chi^{(1)}_{as1}$, and (c) $\chi^{(3)}_{as1,s1}$ plotted against their respective detunings Δ_{s1} or Δ_{as1} in the monochromatic limit of $\gamma_L \to 0$ so that $\Delta_{p10} \equiv \Delta_{p1}$, $\Delta_{p20} \equiv \Delta_{p2}$, and $\Delta_{c0} \equiv \Delta_c$. Other parameters are the same as in Fig. 2 except atomic density $N_0 = 9 \times 10^{11}$ cm^{-3}.

with L being the interaction length while A the area that the Stokes and anti-Stokes photons cross as they propagate in the z direction. Note that we just include $\chi^{(3)}_{as1,s1}$ arising from $\rho^{(1)}_{41}$ in $\hat{H}_I(t)$ because an essential population can be found in state $|1\rangle$ while neglecting the contribution of $\chi^{(3)}_{s1,as1}$ arising from $\rho^{(1)}_{52}$ because state $|2\rangle$ is roughly empty in the 'quasi' dark-state regime. This aligns with the fact that $\chi^{(3)}_{s1,as1}$ has no contributions to the biphoton generation rate given below due to a vanishing contour frequency integration of this complex function in the upper half-plane [27]. In this regime, we have also very weak nonlinear (SFWM) interactions, which make the simultaneous generation of multiple Stokes and anti-Stokes photon pairs unlikely. Within such a weak scattering limit, the well-known first-order term in the dynamic evolution *viz.* $\hat{\mathbb{I}} + \frac{i}{\hbar}\int dt\, \hat{H}_I(t)$ projects the vacuum state $|0\rangle$ onto the general state $|\Psi\rangle \approx |0\rangle + |\Psi\rangle_A + \cdots$, where

$$|\Psi\rangle_A = \int d\omega_{s1} \int d\omega_{as1} \Big[\int d\omega_{p1} f_{p1}(\omega_{p1}) \int d\omega_c f_c(\omega_c) j_A(\dots) \delta(\omega_c + \omega_{p1} - \omega_{s1} - \omega_{as1}) \Big] \hat{a}^\dagger_{s1}(\omega_{s1}) \hat{a}^\dagger_{as1}(\omega_{as1}) |0\rangle. \quad (6)$$

The δ function in $|\Psi\rangle_A$ indicates energy conservation and arises directly from the time-integration of $\hat{H}_I(t)$, following a multi-mode expansion of two *classical* driving fields in terms of complex amplitudes $\{E_{p1}, E_c\}$ and frequency-dependent envelopes $\{f_{p1}, f_c\}$ as well as a standard procedure for the *quantized* Stokes $\hat{E}_{s1}$ and anti-Stokes $\hat{E}_{as1}$ fields [73]. Note also that the product

$$j_A(\dots) = L \times \kappa_A(\dots) \times \Phi_A(\dots), \quad (7)$$

comprises the nonlinear wave-mixing function

$$\kappa_A(\dots) = \frac{\sqrt{\omega_{s1}\omega_{as1}}}{2ic} \chi^{(3)}_{as1,s1} E_{p1} E_c, \quad (8)$$

and the phase-mismatch function

$$\Phi_A(\dots) = \exp\left(-\frac{i\Delta k_A L}{2}\right) \mathrm{sinc}\left(\frac{\Delta k_A L}{2}\right), \quad (9)$$

which arises instead from the space-integration of $\hat{H}_I(t)$. Here, we have denoted by $\Delta k_A = k_{p1} - k_{s1} + k_c - k_{as1}$ the mismatch of wave vectors, including $k_{as1} = \omega_{as1} n_{as1}/c$ with $n_{as1} = (1 + \chi^{(1)}_{as1})^{1/2}$ being the refractive index at the anti-Stokes frequency that is in turn directly related to the linear component of $\rho^{(1)}_{41}$. Similar expressions and discussions hold for k_{p1}, k_{s1}, and k_c. Moreover, $(\dots)$ is a shorthand for all frequency dependencies appearing in the linear and nonlinear components of $\rho^{(1)}_{41}$, required to determine the linear $\chi^{(1)}_{as1}$ and nonlinear $\chi^{(3)}_{as1,s1}$ susceptibilities in Eqs. (8) and (9), hence their product j_A. These explicitly consist of the pump (ω_{p1}), coupling (ω_c) and photon pairs ($\omega_{s1}, \omega_{as1}$) frequency variables besides the set of driving parameters $\mathcal{P}_d$ used in Eq. (2).

We recall that $\hat{H}_I$ in Eq. (5) is an *effective* Hamiltonian, through which we have accounted for the effects of two pump and one coupling linewidths *indirectly* through the linewidth-averaged zeroth-order populations and coherences $\sigma^{(0)}_{ij}$ that contribute to both linear and nonlinear susceptibilities (see Appendix C). That means, we adopt here a description of our atomic sample's optical responses in terms of *dressed* linear and nonlinear susceptibilities because they are built from solutions of Eqs. (C2) that depend on the zeroth-order averages $\sigma^{(0)}_{ij}$ in Sec. III.

Direct linewidth contributions of one pump and the coupling field to photon pair state $|\Psi\rangle_A$, represented by the square-bracket term in Eq. (6), are included by convolving $j_A(\dots)$ with the spectral envelopes $f_{p1}(\omega_{p1})$ and

$f_c(\omega_c)$ under the condition of energy conservation. This yields the joint spectral amplitude (JSA) [35–37],

$$J_A(\omega_{s1},\omega_{as1},\mathcal{P}_d)=\int_{-\infty}^{\infty}d\omega_{p1}\frac{\gamma_{p1}\gamma_c\; j_A(\omega_{p1},\omega_{s1},\omega_{as1},\mathcal{P}_d)}{\pi^2[(\omega_{p1}-\varpi_{p1})^2+\gamma_{p1}^2][(\omega_{s1}+\omega_{as1}-\omega_{p1}-\varpi_c)^2+\gamma_c^2]}, \tag{10}$$

where ω_c has been replaced by $\omega_{s1}+\omega_{as1}-\omega_{p1}$ in the expressions of j_A and f_c. The biphoton state then becomes

$$|\Psi\rangle_A=\int d\omega_{s1}\int d\omega_{as1}J_A(\omega_{s1},\omega_{as1},\mathcal{P}_d)\hat{a}_{s1}^{\dagger}(\omega_{s1})\hat{a}_{as1}^{\dagger}(\omega_{as1})|0\rangle. \tag{11}$$

where J_A gives the degree of spectral correlation between two photons emitted in pair while its square $|J_A|^2$ refers to the joint spectral intensity (JSI), a directly measurable quantity in experiment. For driving beams with vanishing linewdiths $\{\gamma_{p1},\gamma_c\}\to 0$, J_A recovers j_A as a point-wise JSA evaluated at the pump (ϖ_{p1}) and coupling (ϖ_c) central frequencies [38] with the generated biphotons subject to the constraint of $\omega_{s1}+\omega_{as1}\simeq\varpi_{p1}+\varpi_c$ emerging from the δ-function limit of the Lorentzian modulation. For driving beams whose linewidths $\{\gamma_{p1},\gamma_c\}$ are nonzero but sufficiently smaller than the spectral variations of phase-mismatch Φ and wave-mixing κ functions, *i.e.* for Lorentzians that are much narrower than the linear and nonlinear spectral responses, we can still set $\omega_{p1}\to\varpi_{p1}$ and $\omega_c\to\varpi_c$ inside j_A to approximate J_A as

$$\begin{aligned}J_A(\omega_{s1},\omega_{as1},\mathcal{P}_d)&\simeq j_A(\omega_{s1},\omega_{as1},\mathcal{P}_d)\times\int_{-\infty}^{\infty}d\omega_{p1}\frac{\gamma_{p1}\gamma_c}{\pi^2[(\omega_{p1}-\varpi_{p1})^2+\gamma_{p1}^2][(\omega_{s1}+\omega_{as1}-\omega_{p1}-\varpi_c)^2+\gamma_c^2]}\\&=j_A(\omega_{s1},\omega_{as1},\mathcal{P}_d)\times\frac{1}{\pi}\frac{2\gamma_L}{(\omega_{s1}+\omega_{as1}-\varpi_{p1}-\varpi_c)^2+(2\gamma_L)^2}.\end{aligned} \tag{12}$$

The final expression has been obtained by taking $\gamma_{p1}=\gamma_c=\gamma_L$ under a *narrow bandwidth approximation*.

In Fig. 4(a), we plot $|J_A|$ in Eq. (10) as a function of Stokes Δ_{s1} and anti-Stokes Δ_{as1} detunings. Two slender bright regions along the anti-diagonal pinpoint the spectral domains where the ω_{s1} and ω_{as1} photons are most likely to be generated in pair. This is a distinctive feature of the spindle-shaped JSA profile displaying how the ω_{s1} and ω_{as1} photons are spectrally anti-correlated due to energy conservation. Such correlations are crucial for applications that rely on strongly correlated photon pairs. We also introduce in Fig. 4(b) a transformation (rotation) to the overall detuning $\Delta_A=\Delta_{as1}+\Delta_{s1}$ (anti-diagonal direction) to provide a better preview of the results. The *mean* extent of this overall detuning turns out to be approximately $2\gamma_L$ when the pump and coupling beams are resonant ($\Delta_{p10}=\Delta_{c0}=0$) with equal linewidths as considered in Fig. 2. A comparison of panels (b), (c), and (d) reveals that the photon pair's linewidth is primarily determined by γ_L only in certain cases. As γ_L decreases, its influence on shaping the photon pair's linewidth becomes clearly less and less relevant. In particular, panel (d) shows that, while the photon pair's linewidth (FWHM) is approximately $4\times10^{-3}\gamma$, the average overall spread of Δ_A induced by the pump and coupling beams is more than an order of magnitude smaller.

Notice, on the other hand, that the approximation given by Eq. (12) provides a basic understanding into how the common laser linewidth γ_L can influence the overall JSA – $J_A(\omega_{s1},\omega_{as1},\mathcal{P}_d)$. The latter consists in fact of a point-wise function $j_A(\omega_{p1},\omega_{s1},\omega_{as1},\mathcal{P}_d)$ at central frequencies ϖ_{p1} and ϖ_c of two driving beams modulated by a Lorentzian distribution at twice the linewidth $2\gamma_L$, as a result of the convolution integral in the first line of Eq. (12). The linewidth dependence of J_A is therefore tied both to such Lorentzian modulation and to the point-wise function j_A. The former modulation clearly yields a broadening of the peak as the linewidth increases and this closely aligns with the broadening of the spectral amplitude observed at larger γ_L's in Fig. 4. The latter j_A function, primarily governed by the nonlinear susceptibility $\chi^{(3)}_{as1,s1}$, is enhanced instead for larger γ_L's (see Sec. IV). The overall dependence of J_A on γ_L is then governed by the interplay between the Lorentzian modulation and the nonlinear response of the medium. Above, we have considered that the phase-mismatch function Φ_A is largely insensitive to the variations in γ_L (not shown), which is why κ_A and hence j_A basically depends on $\chi^{(3)}_{as1,s1}$.

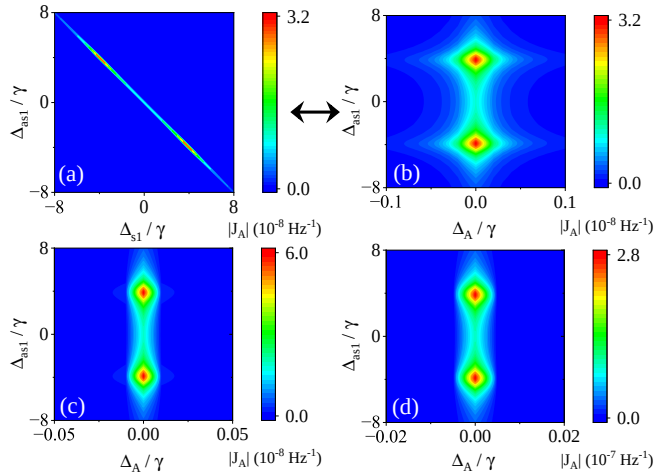

FIG. 4: (a) JSA modulus $|J_A|$ plotted against detunings Δ_{s1} and Δ_{as1}. (b-d) $|J_A|$ plotted against detunings Δ_A and Δ_{as1} after a 45° rotation. The common linewidth of two pump and one coupling beams is set as $\gamma_L = 2\pi \times 20$ kHz (a, b), $2\pi \times 2.0$ kHz (c), and $2\pi \times 0.2$ kHz (d), which result in different detuning scales in panels (b), (c), and (d). Other parameters are the same as in Fig. 3 except $L = 100$ μm.

Next, we consider the intensity correlation function

$$G_A^{(2)}(t_{s1}, t_{as1}) = |\langle 0|\hat{a}_{s1}(t_{s1})\hat{a}_{as1}(t_{as1})|\Psi\rangle_A|^2, \tag{13}$$

between a Stokes photon (ω_{s1}) generated at time t_{s1} and an anti-Stokes photon (ω_{as1}) generated at time t_{as1} [27]. Here, $\hat{a}_j(t_j)$ is an inverse Fourier transformation of the annihilation operator $\hat{a}_j(\omega_j)$ appearing in Eq. (6) with

$$\hat{a}_j(t_j) = \frac{1}{\sqrt{2\pi}} \int d\omega_j \hat{a}_j(\omega_j) e^{-i\omega_j t_j}, \tag{14}$$

and obeys the commutation relation

$$[\hat{a}_j(t_j), \hat{a}_j^\dagger(t_j')] = \delta(t_j - t_j'). \tag{15}$$

With the help of Eq. (11), this intensity correlation function can be written in a more explicit form as

$$G_A^{(2)}(\tau_A) = \frac{L^2}{4\pi^2} \left| \int\int d\omega_{s1} d\omega_{as1} J_A(\omega_{s1}, \omega_{as1}, \mathcal{P}_d) e^{-i(\Delta_{s1} - \Delta_{as1})\tau_A/2} \right|^2, \tag{16}$$

which just depends on the time delay $\tau_A = t_{as1} - t_{s1}$ since our dressed atomic sample is statistically stationary so that the generation of $\{\omega_{s1}, \omega_{as1}\}$ photon pairs is time-translation invariant. The relevant generation rate can finally be computed through $S_A = \int d\tau_A G_A^{(2)}(\tau_A)$.

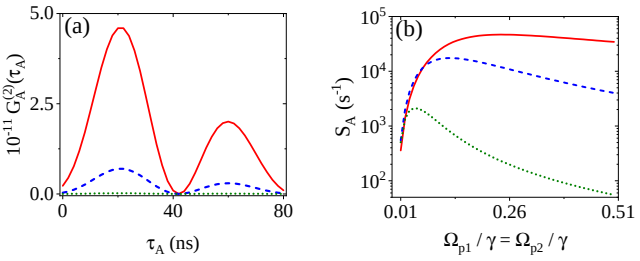

FIG. 5: (a) Intensity correlation function $G_A^{(2)}$ plotted against time delay τ_A and (b) biphoton generation rate S_A plotted against pump Rabi frequencies $\Omega_{p1} = \Omega_{p2}$ for the common laser linewidth γ_L of values $2\pi \times 200$ kHz (red-solid), $2\pi \times 20$ kHz (blue-dashed), and $2\pi \times 2.0$ kHz (green-dotted). Other parameters are the same as in Fig. 4.

Both intensity correlation function $G_A^{(2)}$ and biphoton generation rate S_A have been calculated in Fig. 5 for three different values of the common laser linewidth γ_L. We can see from Fig. 5(a) that $G_A^{(2)}$ exhibits significantly enhanced maximal amplitudes at two specific values of τ_A while keeping roughly unchanged oscillating profiles as γ_L increases from $2\pi \times 2.0$ kHz to $2\pi \times 20$ kHz until $2\pi \times 200$ kHz. In Fig. 5(b), S_A shows a non-monotonic and non-oscillatory dependence on pump Rabi frequencies $\Omega_{p1} = \Omega_{p2}$ and is also significantly enhanced with the increase of γ_L. Moreover, we find that optimal pump Rabi frequencies corresponding to most efficient biphoton generation appear in a wider, flatter, and higher-valued range with the increase of γ_L. Note however that a large enough γ_L may result in a remarkable population transfer outside of the dark state, hence increasing the linear absorption and Raman gain of generated photon pairs (see Fig. 2). In this regard, we need to pursue a balance on achieving efficient biphoton generation and maintaining dark-state stability by carefully controlling γ_L.

VI. INDISTINGUISHABILITY OF TWO SFWM PROCESSES

We have analysed frequency and time correlations of the $\{\omega_{s1}, \omega_{as1}\}$ photon pairs through joint spectral amplitude J_A and intensity correlation function $G_A^{(2)}$, respectively, in Fig. 4 and Fig. 5. Process B can be treated similarly by introducing another joint spectral amplitude J_B

and another intensity correlation function $G_B^{(2)}$, following the same approach as for process A, along with newly defined parameters $\Delta_B = \Delta_{as2} + \Delta_{s2}$ and $\tau_B = t_{as2} - t_{s2}$. It is not difficult to imagine that J_B and $G_B^{(2)}$ would exhibit the same behaviors as J_A and $G_A^{(2)}$, respectively, in the symmetric pump case of $\Omega_{p1} = \Omega_{p2}$ and $\Delta_{p10} = \Delta_{p20}$. We now proceed to identify with numerical analysis the parameter regimes of $\Omega_{p1} \neq \Omega_{p2}$ and $\Delta_{p10} \neq \Delta_{p20}$ where J_A and J_B are still indistinguishable as γ_L is varied, but won't examine the difference between $G_A^{(2)}$ and $G_B^{(2)}$ since it is trivial for comparing processes A and B.

Once again, we consider that states of higher photon numbers can be ignored in the weak spontaneous scattering limit. Then, the overall output state including both process A and process B can be expressed as

$$|\Psi\rangle_{out} \simeq |0\rangle + |\Psi\rangle_A + |\Psi\rangle_B, \tag{17}$$

with the biphoton state for process B being (cf. Eq. (11))

$$|\Psi\rangle_B = \int d\omega_{s2} \int d\omega_{as2} J_B(\omega_{s2}, \omega_{as2}, \mathcal{P}_d) \hat{a}_{s2}^\dagger(\omega_{s2}) \hat{a}_{as2}^\dagger(\omega_{as2}) |0\rangle, \tag{18}$$

where $J_B(\omega_{s2}, \omega_{as2}, \mathcal{P}_d)$ is given by an expression analogous to $J_A(\omega_{s1}, \omega_{as1}, \mathcal{P}_d)$ in Eq. (10) upon a suitable label exchange ($1 \leftrightarrow 2$) for pump fields and photon pairs. The degree of spectral indistinguishability between the photon pairs generated through processes A and B can be assessed by computing the *normalized* mismatch

$$D_J = \frac{|\mathrm{J}_B| - |\mathrm{J}_A|}{|\mathrm{J}_B| + |\mathrm{J}_A|}, \tag{19}$$

with D_J approaching zero indicating best spectral frequency indistinguishability at variance with D_J approaching ± 1 indicating that one process exhibits a significantly different joint spectral intensity than the other. Recall that the quantities directly measurable in experiment are typically the JSI functions $|\mathrm{J}_A|^2$ and $|\mathrm{J}_B|^2$ for processes A and B, respectively. Even when the overall output state $|\Psi\rangle_{out}$ is employed for the heralded generation of color-entangled photons, the relevant figure of merit (*i.e.*, negativity of partial transpose) only depends on $|\mathrm{J}_A|$ and $|\mathrm{J}_B|$ and achieves its maximum value (unity) when $D_J = 0$ [41]. This is why variations of D_J reported in Fig. 6 and Fig. 8 across the two-parameter spaces of pump central detunings and Rabi frequencies are appropriate to offer valuable insights into minimizing spectral differences and hence into the indistinguishability of biphotons created via different SFWM processes. While D_J characterizes the spectral distinguishability between processes A and B, the relative phase of J_A and J_B may also affect their overall indistinguishability. We therefore introduce a normalized phase-sensitive metric, $\tilde{D}_J = |\mathrm{J}_B - \mathrm{J}_A| / \sqrt{|\mathrm{J}_B|^2 + |\mathrm{J}_A|^2}$, whose results are also presented in Fig. 6 and Fig. 8 for comparison.

A. Effects of pump detunings

In order to study the effect of pump detunings (and later on of Rabi frequencies), we fix our attention to J_A for values of Δ_{s1} and Δ_{as1} corresponding to one of the maxima appearing as red spots in Fig. 4, and similarly for J_B, while other choices of Stokes and anti-Stokes frequencies lead to analogous results (another example being discussed in Appendix E). We show in Fig. 6 a detailed analysis of JSA moduli $|J_A|$ and $|J_B|$ along with their normalized mismatch D_J in relation to central detunings Δ_{p10} and Δ_{p20} of the two pumps. It is easy to find from Figs. 6(a) and 6(b) that $|J_A|$ and $|J_B|$ are both nonzero only in a small region centered at $\{\Delta_{p10} = 0, \Delta_{p20} = 0\}$ while their maxima appear around $\{\Delta_{p10} = 0, \Delta_{p20} = \pm 0.05\gamma\}$ and $\{\Delta_{p10} = \pm 0.05\gamma, \Delta_{p20} = 0\}$, respectively. Anyway, $|J_A|$ and $|J_B|$ in their coexisting central region are roughly equal and at most about 5.3 times smaller than their maxima found in orthogonal off-centered regions, indicating thus an essential indistinguishable generation of the $\{\omega_{s1}, \omega_{as1}\}$ and $\{\omega_{s2}, \omega_{as2}\}$ biphotons. The degree of this spectral indistinguishability can be assessed from Fig. 6(c), where we find $D_J \approx 10^{-6}$ at point $(\Delta_{p10}, \Delta_{p20}) = (0, 0)$ and thus have a spectral indistinguishability approaching 100% around this central point. Increasing the common laser linewidth γ_L from $2\pi \times 20$ kHz to $2\pi \times 200$ kHz, we further find from Fig. 6(d) a remarkable change of D_J, which varies within ± 0.93 at the 20 kHz linewidth but within ± 0.1 at the 200 kHz linewidth. This reduction of $|D_J|$ owing to an increase of γ_L not only reflects an enhanced spectral overlap between $|J_A|$ and $|J_B|$ in orthogonal off-centered regions, but also corresponds to a broader coexisting central region where $|J_A|$ and $|J_B|$ remain nearly identical to result in $D_J \to 0$.

It is also clear, upon a close inspection of Figs. 6(c) and 6(d), that a large degree of spectral indistinguishability occurs near both diagonals even for quite large values of $|\Delta_{p20}| \simeq |\Delta_{p10}|$, where $|J_A|$ and $|J_B|$ must exhibit an optimal overlap with minimal variations. Keep in mind, however, that $|J_A|$ and $|J_B|$ become very small when deviating from the coexisting central region along both diagonals so that the corresponding indistinguishability is meaningless since biphotons cannot be efficiently gener-

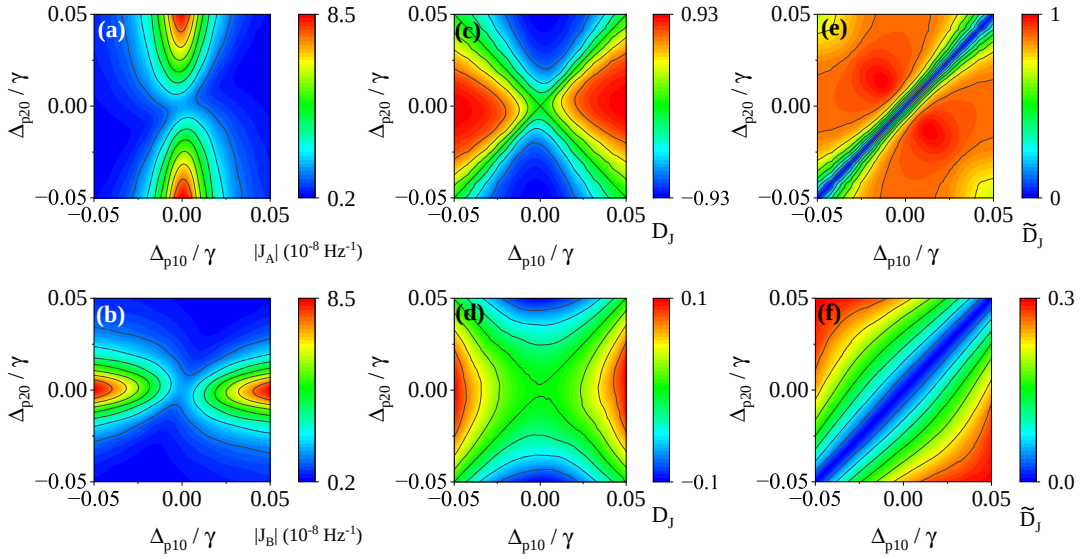

FIG. 6: JSA Moduli $|J_A|$ (a) and $|J_B|$ (b), *Normalized* mismatch D_J (c), *phase-sensitive* mismatch $\tilde{D}_J$ (e) for $\gamma_L = 2\pi \times 20$ kHz plotted against the pumps detuning Δ_{p10} and Δ_{p20}. Same in panels (d,f) for a larger linewidth $\gamma_L = 2\pi \times 200$ kHz. Here we set $\Delta_{as1} = -\Delta_{s1} = 3.9\ \gamma$ and $\Delta_{as2} = -\Delta_{s2} = 3.9\ \gamma$ corresponding to best SFWM efficiency generation respectively for process A and B (See Fig. 4(a)). Other parameters are the same as in Fig. 4.

ated. For comparison, we also show in Figs. 6(e) and 6(f) the phase-sensitive metric $\tilde{D}_J$, which is small only along the main diagonal ($\Delta_{p20} \simeq \Delta_{p10}$) while grows large along the anti-diagonal ($\Delta_{p20} \simeq -\Delta_{p10}$) because here the relative phase between J_A and J_B is close to π. To be more specific, at $(\Delta_{p10}, \Delta_{p20}) = (005\gamma, -005\gamma)$, we have $|D_J| \approx 0.005$ corresponding to a 99.5% indistinguishability just in amplitude but $|\tilde{D}_J| \approx 0.9$ corresponding to a 10% indistinguishability including phase.

Examining the case of two pumps with different central detunings ($\Delta_{p10} \neq \Delta_{p20}$) in Fig. 7, we observe that JSA moduli $|J_A|$ and $|J_B|$, reflecting the joint detection probability spectrum of processes A and B, exhibit a gradual deviation from the complete overlap. While for equal detunings ($\Delta_{p10} = \Delta_{p20}$), $|J_A|$ and $|J_B|$ fully overlap with vanishing values of D_J indicating the optimal indistinguishability, tiny symmetric detunings ($\Delta_{p10} = -\Delta_{p20}$) as in Fig. 7($a_1$) or asymmetric detunings ($\Delta_{p10} \neq -\Delta_{p20}$) as in Fig. 7($b_1$) restricts the spectral overlap to regions around, respectively, $\Delta_{A,B} \simeq \Delta_{p10} + \Delta_{p20} = 0$ and $\Delta_{A,B} \simeq \Delta_{p10} + \Delta_{p20} \neq 0$, where $|J_A|$ and $|J_B|$ are significantly smaller than their maximum values.

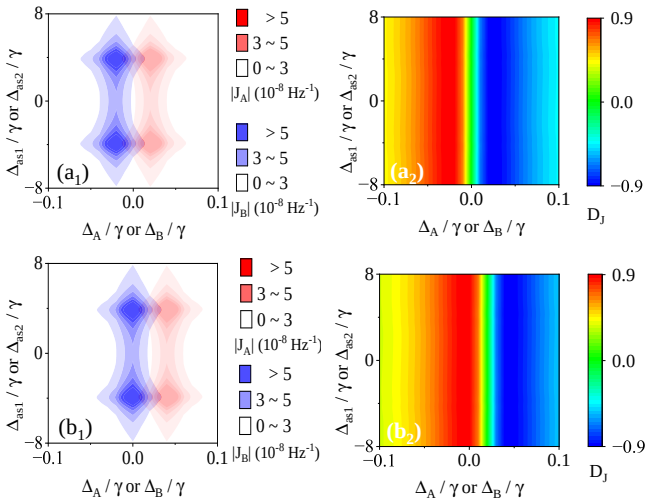

FIG. 7: (a_1) JSA modulus $|J_A|$ (red) plotted against Δ_A and Δ_{as1} and $|J_B|$ (blue) plotted against Δ_B and Δ_{as2} for two narrow pumps ($\gamma_L = 2\pi \times 20$ kHz) *symmetrically* detuned slightly off resonance viz. $\Delta_{p10} = -\Delta_{p20} = 0.02\gamma$. ($b_1$) Same as above for pumps *asymmetrically* detuned viz. $\Delta_{p10} = 0.04\gamma$ and $\Delta_{p20} = 0$. (a_2) Normalised mismatch D_J between $|J_A|$ and $|J_B|$ in (a_1). (b_2) Mismatch D_J for the two JSA's $|J_A|$ and $|J_B|$ in (b_1). Other parameters are the same as in Fig. 4.

B. Effects of pump Rabi frequencies

Next in Figs. 8 we plot $|J_A|$, $|J_B|$ and their corresponding mismatches D_J and $\tilde{D}_J$ against the two pumps Rabi frequencies Ω_{p1} and Ω_{p2}. In Figs. 8(a) and 8(b), the color scale from blue to red indicate increasing values of $|J_A|$ and $|J_B|$, with red areas corresponding to higher probabilities of biphoton generation. It is clear that $|J_A|$ and $|J_B|$ are sensitive to the changes of pump Rabi frequencies and exhibit distinct regions of high and low values. Again, along the diagonal ($\Omega_{p1} = \Omega_{p2}$), the $\{\omega_{s1}, \omega_{as1}\}$ and $\{\omega_{s2}, \omega_{as2}\}$ biphotons exhibit identical generation probabilities, leading thus to $D_J \to 0$ and the optimal spectral indistinguishability as depicted in

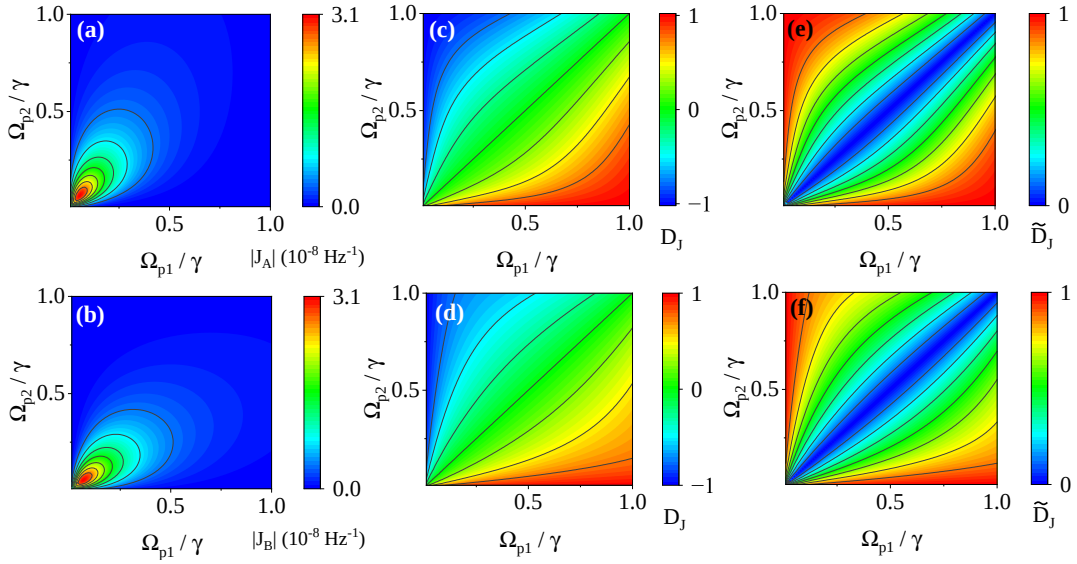

FIG. 8: Same as in Fig. 6 for the moduli $|J_A|$ (a) and $|J_B|$ (b), their *normalized* mismatch D_J (c,d) and *phase-sensitive* mismatch $\tilde{D}_J$ (e,f) yet plotted here against pump Rabi frequencies Ω_{p1} and Ω_{p2}.

Figs. 8(c) and 8(d). The corresponding phase-sensitive metric $\tilde{D}_J$ displayed in Figs. 8(e) and 8(f) varies between 0 and 1 and follows the same overall trend as D_J, *i.e.*, approaching zero along the diagonal where the two JSAs keep roughly equal in both amplitude and phase. Deviating from the diagonal, *e.g.*, with $\Omega_{p1} = \gamma/3$ and $\Omega_{p2} = \gamma/6$, the two metrics become evidently nonzero to different extents, giving $|D_J| \approx 0.25$ (a 75% degree of indistinguishability) and $|\tilde{D}_J| \approx 0.34$ (a 66% degree of indistinguishability). Note also that, with the increase of laser linewidth γ_L from 20 kHz to 200 kHz, the overall distributions of both D_J and $\tilde{D}_J$ become slightly narrower, although rather good spectral indistinguishability is still maintained close to the diagonal. In this regime, the phase contribution appears minor, and amplitude matching remains the dominant factor determining the spectral overlap between the two SFWM processes.

With equal pump Rabi frequencies $\Omega_{p1} = \Omega_{p2}$ as considered in Fig. 4, JSA moduli $|J_A|$ and $|J_B|$ should fully overlap to result in the optimal indistinguishability with $D_J \to 0$ for all frequency components of the $\{\omega_{s1}, \omega_{as1}\}$ and $\{\omega_{s2}, \omega_{as2}\}$ biphotons. In another case of $\Omega_{p1} \neq \Omega_{p2}$, however, we can see from Fig. 9 that the spectral distributions of $|J_A|$ and $|J_B|$ turn out to be different in width though their centers and shapes remain similar, restricting thus the indistinguishability to only partial frequency components of the $\{\omega_{s1}, \omega_{as1}\}$ and $\{\omega_{s2}, \omega_{as2}\}$ biphotons. To be more specific, due to $\Omega_{p1} > \Omega_{p2}$ as considered here, the $\{\omega_{s1}, \omega_{as1}\}$ biphoton can be generated in a wider region with a lower probability than the $\{\omega_{s2}, \omega_{as2}\}$ biphoton because $|J_A|$ exhibits a wider profile and a lower amplitude than $|J_B|$. This makes D_J no longer vanishing for all frequency components of the paired biphotons generated via two different SFWM processes.

VII. CONCLUSIONS

In summary, we have proposed an effective scheme for generating a pair of indistinguishable biphotons via *dual* SFWM processes in specific five-level cold atoms driven by realistic laser sources. The accurate characterization of Lorentzian spectral profiles for three driving beams not only provides practical estimates of the atomic interface's optical responses including populations and coherences, but also offers a straightforward way to control the JSA moduli $|J_A|$ and $|J_B|$ and further quantify their normalized mismatch D_J and the phase-sensitive metric $\tilde{D}_J$. Unlike crystal nonlinearities typically characterised by frequency-independent susceptibilities, in our atomic scheme the nonlinear optical responses to two Stokes and two anti-Stokes components of the paired biphotons strongly depend on corresponding frequencies. Accordingly, $|J_A|$ and $|J_B|$ exhibit a significant spectral overlap to yield a good spectral indistinguishability under specific atomic sample preparation and driving conditions, among which the most important one may be the narrow-linewidth approximation of diving beams. In the case of two resonant ($\Delta_{p10} = \Delta_{p20}$) and balanced ($\Omega_{p1} = \Omega_{p2}$) pumps, for instance, we find that $D_J \to 0$ and $\tilde{D}_J \to 0$ while both $|J_A|$ and $|J_B|$ remain appreciable, *e.g.*, on the order of 10^{-8} Hz^{-1}, confirming an efficient generation of photon pairs with a concomitant large degree (up to 100%) of the spectral indistinguishability. Increasing the linewidths of driving beams enlarges the parameter region where the indistinguishability occurs, though this must be balanced against enhanced linear absorption and Raman gain associated with excessive broadening.

Biphoton sources are basic building blocks for achieving the required photon indistinguishability in heralding schemes. For instance, the large degree of biphoton in-

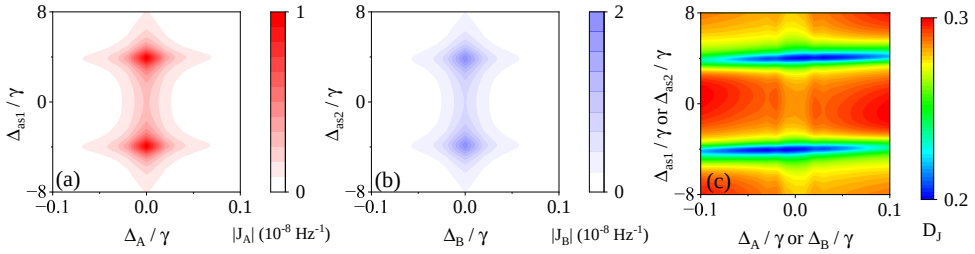

FIG. 9: JSA modulus $|J_A|$ plotted against Δ_A and Δ_{as1} (a) as well as $|J_B|$ against Δ_B and Δ_{as2} (b) along with their normalized mismatch D_J (c) for $\gamma_L = 2\pi \times 20$ kHz. Other parameters are the same as in Fig. 4 except $\Omega_{p1} = \gamma/3$ and $\Omega_{p2} = \gamma/6$.

distinguishability observed here can be harnessed to obtain highly indistinguishable single photons via heralding messages [74] or coherent and tunable heralded single-photon entanglement [41]. Both of them are essential for applications in quantum communications [48] and information processing [75]. Since SFWM third-order nonlinearities underpin modern integrated photonics research, our scheme are desired to be extended to hybrid photonic interfaces, provided they exhibit a comparable five-level *dual*-SFWM configuration. Our scheme may further be generalized to generate more than a pair of biphotons by considering suitable multi-level atomic manifolds.

ACKNOWLEDGMENTS

This work is supported by the National Natural Science Foundation of China (Grant No. 62375047), the Italian PNRR MUR (Grant No. PE0000023-NQSTI), the Natural Science Foundation of Hebei Province (Grant No. A2025205028), and the Science Foundation of Hebei Normal University of China (Grant No. L2025B11).

APPENDIX A: QUANTUM-LANGEVIN APPROACH

Here we show how finite laser linewidths can be included with a quantum-Langevin approach by focusing on the Λ subsystem composed of levels $|1\rangle$, $|3\rangle$, and $|5\rangle$. We first write down the Heisenberg-Langevin equation

$$\begin{aligned}
\partial_t\hat{\sigma}_{11} &= \Gamma_{51}\hat{\sigma}_{55} - i\Omega_{p1}\hat{\sigma}_{15} + i\Omega_{p1}^*\hat{\sigma}_{51},\\
\partial_t\hat{\sigma}_{33} &= \Gamma_{53}\hat{\sigma}_{55} - i\Omega_{p2}\hat{\sigma}_{35} + i\Omega_{p2}^*\hat{\sigma}_{53},\\
\partial_t\hat{\sigma}_{51} &= -(\gamma_{51} - i\Delta_{p1})\hat{\sigma}_{51} + i\Omega_{p1}(\hat{\sigma}_{11} - \hat{\sigma}_{55}) + i\Omega_{p2}\hat{\sigma}_{31},\\
\partial_t\hat{\sigma}_{53} &= -(\gamma_{53} - i\Delta_{p2})\hat{\sigma}_{53} + i\Omega_{p1}\hat{\sigma}_{13} + i\Omega_{p2}(\hat{\sigma}_{33} - \hat{\sigma}_{55}),\\
\partial_t\hat{\sigma}_{31} &= -(\gamma_{31} - i\Delta_{p1} + i\Delta_{p2})\hat{\sigma}_{31} - i\Omega_{p1}\hat{\sigma}_{35} + i\Omega_{p2}^*\hat{\sigma}_{51},
\end{aligned} \tag{A1}$$

restricted by $\hat{\sigma}_{11} + \hat{\sigma}_{33} + \hat{\sigma}_{55} = \mathbb{I}$ and $\hat{\sigma}_{ij} = \hat{\sigma}_{ji}^\dagger$ as usual. By taking $\Omega_{p1} \to \Omega_{p1}e^{i\phi_{p1}}$, $\Omega_{p2} \to \Omega_{p2}e^{i\phi_{p2}}$, $\hat{\sigma}_{51} \to \hat{\sigma}_{51}e^{i\phi_{p1}}$, $\hat{\sigma}_{53} \to \hat{\sigma}_{53}e^{i\phi_{p2}}$, $\hat{\sigma}_{31} \to \hat{\sigma}_{31}e^{i(\phi_{p1}-\phi_{p2})}$, $\hat{\sigma}_{33} \to \hat{\sigma}_{33}$, $\hat{\sigma}_{22} \to \hat{\sigma}_{22}$, and $\hat{\sigma}_{11} \to \hat{\sigma}_{11}$ in above equations to consider the laser linewidths arising from free diffusions in phases $\phi_{p1}(\mathrm{t})$ and $\phi_{p2}(\mathrm{t})$, we further obtain

$$\begin{aligned}
\partial_t\hat{\sigma}_{11} &= \Gamma_{51}\hat{\sigma}_{55} - i\Omega_{p1}\hat{\sigma}_{15} + i\Omega_{p1}^*\hat{\sigma}_{51},\\
\partial_t\hat{\sigma}_{33} &= \Gamma_{53}\hat{\sigma}_{55} - i\Omega_{p2}\hat{\sigma}_{35} + i\Omega_{p2}^*\hat{\sigma}_{53},\\
\partial_t\hat{\sigma}_{51} &= -[\gamma_{51} - i\Delta_{p1} + i\mu_{p1}(t)]\hat{\sigma}_{51} + i\Omega_{p1}(\hat{\sigma}_{11} - \hat{\sigma}_{55}) + i\Omega_{p2}\hat{\sigma}_{31},\\
\partial_t\hat{\sigma}_{53} &= -[\gamma_{53} - i\Delta_{p2} + i\mu_{p2}(t)]\hat{\sigma}_{53} + i\Omega_{p1}\hat{\sigma}_{13} + i\Omega_{p2}(\hat{\sigma}_{33} - \hat{\sigma}_{55}),\\
\partial_t\hat{\sigma}_{31} &= -[\gamma_{31} - i\Delta_{p1} + i\Delta_{p2} + i\mu_{p1}(t) - i\mu_{p2}(t)]\hat{\sigma}_{31} - i\Omega_{p1}\hat{\sigma}_{35} + i\Omega_{p2}^*\hat{\sigma}_{51},
\end{aligned} \tag{A2}$$

where we have considered that $\partial_t\phi_{pj}(t) = \mu_{pj}(t)$ with $\mu_{pj}(t)$ being the δ-correlated Langevin-noise operators. The free-diffusion coefficients of these operators are determined by half laser linewidths γ_{pj} via $\langle\mu_{pj}(t)\mu_{pj}(t')\rangle = \gamma_{pj}\delta(t-t')$ corresponding to the typical Lorentzian spectral profiles described by

$$f(\omega_{pj}) = \frac{1}{\pi}\frac{\gamma_{pj}}{(\omega_{pj} - \varpi_{pj})^2 + \gamma_{pj}^2} \tag{A3}$$

where ω_{pj} and ϖ_{pj} denote the carrier and central frequencies, respectively.

Then we try to get the semiclassical solutions by taking $\rho_{ij}=\langle\sigma_{ij}\rangle$ as the mean values of relevant transition ($i\neq j$) or projection ($i=j$) operators. With this consideration, Eq. (A2) can be cast into

$$\begin{aligned}
\partial_t\rho_{11} &= \Gamma_{51}\rho_{55}-i\Omega_{p1}\rho_{15}+i\Omega_{p1}^*\rho_{51},\\
\partial_t\rho_{33} &= \Gamma_{53}\rho_{55}-i\Omega_{p2}\rho_{35}+i\Omega_{p2}^*\rho_{53},\\
\partial_t\rho_{51} &= -(\gamma_{51}-i\Delta_{p1})\rho_{51}+i\langle\mu_{p1}(t)\hat{\sigma}_{51}\rangle+i\Omega_{p1}(\rho_{11}-\rho_{55})+i\Omega_{p2}\rho_{31},\\
\partial_t\rho_{53} &= -(\gamma_{53}-i\Delta_{p2})\rho_{53}+i\langle\mu_{p2}(t)\hat{\sigma}_{53}\rangle+i\Omega_{p1}\rho_{13}+i\Omega_{p2}(\rho_{33}-\rho_{55}),\\
\partial_t\rho_{31} &= -(\gamma_{31}-i\Delta_{p1}+i\Delta_{p2})\rho_{31}+i\langle[\mu_{p1}(t)-\mu_{p2}(t)]\hat{\sigma}_{31}\rangle-i\Omega_{p1}\rho_{35}+i\Omega_{p2}^*\rho_{51},
\end{aligned}\tag{A4}$$

where three terms including $\mu_{p1}(t)$ and/or $\mu_{p2}(t)$ are undetermined yet. These terms can be calculated through the formal integrations of Eq. (A2) multiplied by $\mu_{p1}(t)$, $\mu_{p2}(t)$, or $\mu_{p1}(t)-\mu_{p2}(t)$, i.e.

$$\begin{aligned}
i\langle\mu_{p1}(t)\hat{\sigma}_{51}\rangle &= -\int_0^t dt'\langle\mu_{p1}(t)\mu_{p1}(t')\hat{\sigma}_{51}(t')\rangle\simeq-\int_0^t dt'\langle\mu_{p1}(t)\mu_{p1}(t')\rangle\langle\hat{\sigma}_{51}(t')\rangle=-\gamma_{p1}\rho_{51}(t),\\
i\langle\mu_{p2}(t)\hat{\sigma}_{53}\rangle &= -\int_0^t dt'\langle\mu_{p2}(t)\mu_{p2}(t')\hat{\sigma}_{53}(t')\rangle\simeq-\int_0^t dt'\langle\mu_{p2}(t)\mu_{p2}(t')\rangle\langle\hat{\sigma}_{53}(t')\rangle=-\gamma_{p2}\rho_{53}(t),\\
i\langle[\mu_{p1}(t)-\mu_{p2}(t)]\hat{\sigma}_{31}\rangle &= -\int_0^t dt'[\langle\mu_{p1}(t)-\mu_{p2}(t)][\mu_{p1}(t')-\mu_{p2}(t')]\hat{\sigma}_{31}(t')\rangle\simeq-(\gamma_{p1}+\gamma_{p2}-\gamma_{p1,p2}-\gamma_{p2,p1})\rho_{31}(t),
\end{aligned}\tag{A5}$$

where we have (i) $\gamma_{p1,p2}=\gamma_{p2,p1}=0$ for two completely independent pump fields while (ii) $\gamma_{p1}=\gamma_{p2}=\gamma_{p1,p2}=\gamma_{p2,p1}$ for two completely correlated pump fields. In case (ii) of our interest, Eq. (A4) turns out to be

$$\begin{aligned}
\partial_t\rho_{11} &= \Gamma_{51}\rho_{55}-i\Omega_{p1}\rho_{15}+i\Omega_{p1}^*\rho_{51},\\
\partial_t\rho_{33} &= \Gamma_{53}\rho_{55}-i\Omega_{p2}\rho_{35}+i\Omega_{p2}^*\rho_{53},\\
\partial_t\rho_{51} &= -(\gamma_{51}+\gamma_{p1}-i\Delta_{p1})\rho_{51}+i\Omega_{p1}(\rho_{11}-\rho_{55})+i\Omega_{p2}\rho_{31},\\
\partial_t\rho_{53} &= -(\gamma_{53}+\gamma_{p2}-i\Delta_{p2})\rho_{53}+i\Omega_{p1}\rho_{13}+i\Omega_{p2}(\rho_{33}-\rho_{55}),\\
\partial_t\rho_{31} &= -(\gamma_{31}-i\Delta_{p1}+i\Delta_{p2})\rho_{31}-i\Omega_{p1}\rho_{35}+i\Omega_{p2}^*\rho_{51},
\end{aligned}\tag{A6}$$

with which we can examine steady solutions $\rho_{ij}(\varpi_{p1}+i\gamma_{p1},\varpi_{p2}+i\gamma_{p2})$ of the three-level Λ system by setting $\partial_t\rho_{ij}=0$.

These solutions can also be attained from the two-fold convolutions of $\rho_{ij}(\omega_{p1},\omega_{p2})$ calculated assuming zero laser linewidths with the corresponding spectral profiles $f(\omega_{p1})$ and $f(\omega_{p2})$, i.e.

$$\begin{aligned}
&\rho_{ij}(\varpi_{p1}+i\gamma_{p1},\varpi_{p2}+i\gamma_{p2})=\int_{-\infty}^{\infty}d\omega_{p1}f(\omega_{p1})\int_{-\infty}^{\infty}d\omega_{p2}f(\omega_{p2})\rho_{ij}(\omega_{p1},\omega_{p2})\\
&=\frac{1}{\pi^2}\int_{-\infty}^{\infty}\int_{-\infty}^{\infty}d\omega_{p1}d\omega_{p2}\frac{\gamma_{p1}\gamma_{p2}\rho_{ij}(\omega_{p1},\omega_{p2})}{[(\omega_{p1}-\varpi_{p1})^2+\gamma_{p1}^2][(\omega_{p2}-\varpi_{p2})^2+\gamma_{p2}^2]},
\end{aligned}\tag{A7}$$

valid when ρ_{ij} is analytic in the upper half planes of ω_{p1} and ω_{p2}. This verifies that the free-diffusion coefficients of phases $\phi_{pj}(t)$ are exactly half laser linewidths referring to Lorentzian spectral profiles $f(\omega_{pj})$ [57]. Note however that the quantum-Langevin approach becomes intractable when the full five level system is considered due to the complex interplay among various carrier frequencies, whereas the latter convolution approach is used in the main text to account for the statistically mean effects of finite laser linewidths.

APPENDIX B: ZEROTH-ORDER SOLUTIONS DERIVED FROM DENSITY MATRIX EQUATIONS

Given the weakness of the four generated Stokes and anti-Stokes fields, the zeroth-order solutions for our five-level system is attainable when exclusively accounting for three applied fields. The interaction Hamiltonian, considering the electric-dipole and rotating-wave approximation without the four generated fields, can be rewritten as

$$H_0/\hbar=-(\Delta_{p2}-\Delta_{p1})|3\rangle\langle 3|+\Delta_c|4\rangle\langle 4|+\Delta_{p1}|5\rangle\langle 5|-(\Omega_{p1}|5\rangle\langle 1|+\Omega_{p2}|5\rangle\langle 3|+\Omega_c|4\rangle\langle 2|+H.c.),\tag{B1}$$

satisfying the commutation relation $i\hbar\partial_t\rho_{ij}^{(0)}=[H_0,\rho_{ij}^{(0)}]$. The equations for the five-level system depend on 25 density matrix elements, denoted as ρ_{ij}, where i and j take values from $\{1,2,3,4,5\}$, corresponding to atomic populations

$(i=j)$ or coherences $(i\neq j)$,

$$
\begin{aligned}
\partial_t\rho_{11}^{(0)} &= \Gamma_{51}\rho_{55}^{(0)} + \Gamma_{41}\rho_{44}^{(0)} + i\Omega_{p1}^{*}\rho_{51}^{(0)} - i\Omega_{p1}\rho_{15}^{(0)},\\
\partial_t\rho_{22}^{(0)} &= \Gamma_{52}\rho_{55}^{(0)} + \Gamma_{42}\rho_{44}^{(0)} + i\Omega_{c}^{*}\rho_{42}^{(0)} - i\Omega_{c}\rho_{24}^{(0)},\\
\partial_t\rho_{33}^{(0)} &= \Gamma_{53}\rho_{55}^{(0)} + \Gamma_{43}\rho_{44}^{(0)} - i\Omega_{p2}\rho_{35}^{(0)} + i\Omega_{p2}^{*}\rho_{53}^{(0)},\\
\partial_t\rho_{44}^{(0)} &= -(\Gamma_{41}+\Gamma_{42}+\Gamma_{43})\rho_{44}^{(0)} + i\Omega_{c}\rho_{24}^{(0)} - i\Omega_{c}^{*}\rho_{42}^{(0)},\\
\partial_t\rho_{54}^{(0)} &= -g_{54}\rho_{54}^{(0)} + i\Omega_{p1}\rho_{14}^{(0)} + i\Omega_{p2}\rho_{34}^{(0)} - i\Omega_{c}^{*}\rho_{52}^{(0)},\\
\partial_t\rho_{53}^{(0)} &= -g_{53}\rho_{53}^{(0)} + i\Omega_{p1}\rho_{13}^{(0)} + i\Omega_{p2}\left(\rho_{33}^{(0)} - \rho_{55}^{(0)}\right),\\
\partial_t\rho_{52}^{(0)} &= -g_{52}\rho_{52}^{(0)} + i\Omega_{p1}\rho_{12}^{(0)} + i\Omega_{p2}\rho_{32}^{(0)} - i\Omega_{c}\rho_{54}^{(0)},\\
\partial_t\rho_{51}^{(0)} &= -g_{51}\rho_{51}^{(0)} + i\Omega_{p1}\left(\rho_{11}^{(0)} - \rho_{55}^{(0)}\right) + i\Omega_{p2}\rho_{31}^{(0)},\\
\partial_t\rho_{43}^{(0)} &= -g_{43}\rho_{43}^{(0)} + i\Omega_{c}\rho_{23}^{(0)} - i\Omega_{p2}\rho_{45}^{(0)},\\
\partial_t\rho_{42}^{(0)} &= -g_{42}\rho_{42}^{(0)} + i\Omega_{c}\left(\rho_{22}^{(0)} - \rho_{44}^{(0)}\right),\\
\partial_t\rho_{41}^{(0)} &= -g_{41}\rho_{41}^{(0)} - i\Omega_{p1}\rho_{45}^{(0)} + i\Omega_{c}\rho_{21}^{(0)},\\
\partial_t\rho_{32}^{(0)} &= -g_{32}\rho_{32}^{(0)} + i\Omega_{p2}^{*}\rho_{52}^{(0)} - i\Omega_{c}\rho_{34}^{(0)},\\
\partial_t\rho_{31}^{(0)} &= -g_{31}\rho_{31}^{(0)} + i\Omega_{p2}^{*}\rho_{51}^{(0)} - i\Omega_{p1}\rho_{35}^{(0)},\\
\partial_t\rho_{21}^{(0)} &= -g_{21}\rho_{21}^{(0)} + i\Omega_{c}^{*}\rho_{41}^{(0)} - i\Omega_{p1}\rho_{25}^{(0)},
\end{aligned}
\tag{B2}
$$

restricted by $\rho_{ij}^{(0)} = \rho_{ji}^{(0)*}$ and $\sum_i \rho_{ii}^{(0)} = 1$. Γ_{ij} denotes the population decay rate from level $|i\rangle$ to $|j\rangle$. The respective complex decay rates are defined as follows: $g_{54} = \gamma_{54} + i\left(\Delta_c - \Delta_{p1}\right), g_{53} = \gamma_{53} + i\Delta_{p2}, g_{52} = \gamma_{52} + i\Delta_{p1}, g_{51} = \gamma_{51} + i\Delta_{p1}, g_{43} = \gamma_{43} + i\left(\Delta_c - \Delta_{p1} + \Delta_{p2}\right), g_{42} = \gamma_{42} + i\Delta_c, g_{41} = \gamma_{41} + i\Delta_c, g_{32} = \gamma_{32} + i\left(\Delta_{p1} - \Delta_{p2}\right), g_{31} = \gamma_{31} + i\left(\Delta_{p1} - \Delta_{p2}\right)$ and $g_{21} = \gamma_{21}$.

APPENDIX C: HAMILTONIANS AND DYNAMIC EQUATIONS FOR SFWM PROCESS A

In the specific context of the present work, pair generation takes place through a five-level open interaction loop, where transitions occur sequentially without forming a closed loop. This five-level open-loop driven system may nevertheless be treated as a combination of two four-level closed interaction loops A and B that share two excited states ($|4\rangle$ and $|5\rangle$), the ground $|2\rangle$ and the coupling beam, each subsystem implementing a familiar SFWM process [27]. They are depicted respectively by blue and red transitions in Fig. 1.

It turns out that the two processes influence each other primarily through the Stokes channel, where the photon ω_{s2} (process B), *e.g.*, can impact process A via their shared transition, particularly when Stokes photons are nearly resonant (with that transition). The quasi-dark state trapping regime adopted here (see Sec. III and Sec. IV) minimizes however population redistribution among all five levels, further effectively suppressing spontaneous emission, intrinsically rather weak, from the excited state $|5\rangle$. In the end, this effectively makes our five-level system to behave dynamically as two nearly independent/weakly interacting four-wave mixing SFWM processes depicted respectively by blue (A) and red (B) color transitions in Fig. 1. Within this type of approximation, the effective Hamiltonian for the generation of the photon-pair $\{\omega_{s1}, \omega_{as1}\}$ can be written as

$$
H_A/\hbar = (\Delta_{p1} - \Delta_{s1})|2\rangle\langle 2| + \Delta_{as1}|4\rangle\langle 4| + \Delta_{p1}|5\rangle\langle 5| - (\Omega_{p1}|5\rangle\langle 1| + \Omega_c|4\rangle\langle 2| + \Omega_{s1}|5\rangle\langle 2| + \Omega_{as1}|4\rangle\langle 1| + H.c.). \tag{C1}
$$

The spontaneously emitted Stokes ω_{s1} and anti-Stokes ω_{as1} photon field strengths are relatively weak with respect to the driving fields Ω_{p1} and Ω_c, so we can describe their generation adopting a perturbative approach with respect to the Stokes and anti-Stokes field strengths. Upon inserting H_A into the relevant master equations and with the help of the zeroth-order averaged populations and coherences ($\sigma_{ij}^{(0)}$), yields the following set of equations for the first-order

density matrix elements $\rho_{ij}^{(1)}$:

$$\begin{aligned}
\partial_t\rho_{54}^{(1)} =& -g_{54}^A\rho_{54}^{(1)} + i\Omega_{p1}\rho_{14}^{(1)} - i\Omega_c^*\rho_{52}^{(1)} + i\Omega_{s1}\sigma_{24}^{(0)} - i\Omega_{as1}^*\sigma_{51}^{(0)},\\
\partial_t\rho_{52}^{(1)} =& -g_{52}^A\rho_{52}^{(1)} + i\Omega_{p1}\rho_{12}^{(1)} - i\Omega_c\rho_{54}^{(1)} + i\Omega_{s1}\left(\sigma_{22}^{(0)} - \sigma_{55}^{(0)}\right),\\
\partial_t\rho_{51}^{(1)} =& -g_{51}^A\rho_{51}^{(1)} + i\Omega_{p1}\left(\rho_{11}^{(1)} - \rho_{55}^{(1)}\right) + i\Omega_{s1}\sigma_{21}^{(0)} - i\Omega_{as1}\sigma_{54}^{(0)},\\
\partial_t\rho_{42}^{(1)} =& -g_{42}^A\rho_{42}^{(1)} + i\Omega_c\left(\rho_{22}^{(1)} - \rho_{44}^{(1)}\right) + i\Omega_{as1}\sigma_{12}^{(0)} - i\Omega_{s1}\sigma_{45}^{(0)},\\
\partial_t\rho_{41}^{(1)} =& -g_{41}^A\rho_{41}^{(1)} - i\Omega_{p1}\rho_{45}^{(1)} + i\Omega_c\rho_{21}^{(1)} + i\Omega_{as1}\left(\sigma_{11}^{(0)} - \sigma_{44}^{(0)}\right),\\
\partial_t\rho_{21}^{(1)} =& -g_{21}^A\rho_{21}^{(1)} - i\Omega_{p1}\rho_{25}^{(1)} + i\Omega_c^*\rho_{41}^{(1)} - i\Omega_{as1}\sigma_{24}^{(0)} + i\Omega_{s1}^*\sigma_{51}^{(0)},
\end{aligned} \tag{C2}$$

with respective complex decay rates are defined as follows: $g_{54}^A = \gamma_{54} + i\left(\Delta_{p1} - \Delta_{as1}\right), g_{52}^A = \gamma_{52} + i\Delta_{s1}, g_{51}^A = \gamma_{51} + i\Delta_{p1}, g_{42}^A = \gamma_{42} + i\left(\Delta_{as1} - \Delta_{p1} + \Delta_{s1}\right), g_{41}^A = \gamma_{41} + i\Delta_{as1}$, and $g_{21}^A = \gamma_{21} + i\left(\Delta_{p1} - \Delta_{s1}\right)$. For the anti-Stokes transition channel, the steady-state first-order solutions $\rho_{ij}^{(1)}$ ($\partial_t\rho_{ij}^{(1)} = 0$), when appropriately decomposed into contributions from the linear and nonlinear contribution, yield

$$\rho_{41}^{(1)} = \rho_{41}^L E_{as1} + \rho_{41}^{NL} E_{p1} E_c E_{s1}^\dagger, \tag{C3a}$$

where ρ_{41}^L and ρ_{41}^{NL} correspond to the linear and nonlinear responses, respectively. The corresponding linear and third-order nonlinear susceptibilities are given by:

$$\chi_{as1}^{(1)} = \frac{N_0 d_{14}^2}{\hbar\epsilon_0}\rho_{41}^L, \quad \chi_{as1,s1}^{(3)} = \frac{N_0 d_{25} d_{15} d_{14} d_{24}}{4\hbar^3\epsilon_0}\rho_{41}^{NL}. \tag{C3b}$$

Similarly, for the Stokes channel, the first-order coherences are given by:

$$\rho_{52}^{(1)} = \rho_{52}^L E_{s1} + \rho_{52}^{NL} E_{p1} E_c E_{as1}^\dagger. \tag{C4a}$$

The corresponding linear and third-order nonlinear susceptibilities are:

$$\chi_{s1}^{(1)} = \frac{N_0 d_{25}^2}{\hbar\epsilon_0}\rho_{52}^L, \quad \chi_{s1,as1}^{(3)} = \frac{N_0 d_{25} d_{15} d_{14} d_{24}}{4\hbar^3\epsilon_0}\rho_{52}^{NL}. \tag{C4b}$$

APPENDIX D: HAMILTONIANS AND DYNAMIC EQUATIONS FOR SFWM PROCESS B

Similarly, the effective Hamiltonian for the generation of the other photon-pair $\{\omega_{s2}, \omega_{as2}\}$ is

$$H_B/\hbar = (\Delta_{p2} - \Delta_{s2})|2\rangle\langle 2| + \Delta_{as2}|4\rangle\langle 4| + \Delta_{p2}|5\rangle\langle 5| - (\Omega_{p2}|5\rangle\langle 3| + \Omega_c|4\rangle\langle 2| + \Omega_{s2}|5\rangle\langle 2| + \Omega_{as2}|4\rangle\langle 3| + H.c.). \tag{D1}$$

The first-order equations in process B also depend on the zeroth-order solutions,

$$\begin{aligned}
\partial_t\rho_{54}^{(1)} =& -g_{54}^B\rho_{54}^{(1)} + i\Omega_{p2}\rho_{34}^{(1)} - i\Omega_c^*\rho_{52}^{(1)} + i\Omega_{s2}\sigma_{24}^{(0)} - i\Omega_{as2}^*\sigma_{53}^{(0)},\\
\partial_t\rho_{53}^{(1)} =& -g_{53}^B\rho_{53}^{(1)} + i\Omega_{p2}\left(\rho_{33}^{(1)} - \rho_{55}^{(1)}\right) - i\Omega_{as2}\sigma_{54}^{(0)} + i\Omega_{s2}\sigma_{23}^{(0)},\\
\partial_t\rho_{52}^{(1)} =& -g_{52}^B\rho_{52}^{(1)} + i\Omega_{p2}\rho_{32}^{(1)} - i\Omega_c\rho_{54}^{(1)} + i\Omega_{s2}\left(\sigma_{22}^{(0)} - \sigma_{55}^{(0)}\right),\\
\partial_t\rho_{43}^{(1)} =& -g_{43}^B\rho_{43}^{(1)} + i\Omega_c\rho_{23}^{(1)} - i\Omega_{p2}\rho_{45}^{(1)} + i\Omega_{as2}\left(\sigma_{33}^{(0)} - \sigma_{44}^{(0)}\right),\\
\partial_t\rho_{42}^{(1)} =& -g_{42}^B\rho_{42}^{(1)} + i\Omega_c\left(\rho_{22}^{(1)} - \rho_{44}^{(1)}\right) + i\Omega_{as2}\sigma_{32}^{(0)} - i\Omega_{s2}\sigma_{45}^{(0)},\\
\partial_t\rho_{32}^{(1)} =& -g_{32}^B\rho_{32}^{(1)} + i\Omega_{p2}^*\rho_{52}^{(1)} - i\Omega_c\rho_{34}^{(1)} - i\Omega_{s2}\sigma_{35}^{(0)} + i\Omega_{as2}^*\sigma_{42}^{(0)},
\end{aligned} \tag{D2}$$

with respective complex decay rates are defined as follows: $g_{54}^B = \gamma_{54} + i\left(\Delta_{p2} - \Delta_{as2}\right), g_{53}^B = \gamma_{53} + i\Delta_{p2}, g_{52}^B = \gamma_{52} + i\Delta_{s2}, g_{43}^B = \gamma_{43} + i\Delta_{as2}, g_{42}^B = \gamma_{42} + i\left(\Delta_{as2} - \Delta_{p2} + \Delta_{s2}\right)$, and $g_{32}^B = \gamma_{32} + i\left(\Delta_{s2} - \Delta_{p2}\right)$.

Finally, it is worth reiterating that, within our framework, both SFWM processes are based on the same *zero-order* perturbative solutions $\sigma_{ij}^{(0)}$ as Lorentzian averages of $\rho_{ij}^{(0)}$ (see Eq. (2) in the main text).

APPENDIX E: JOINT SPECTRAL INTENSITY MAPS EVALUATED AT VARIOUS EMITTED-PHOTON FREQUENCIES

In Fig. 6 and Fig. 8 of the main text, we have chosen the Stokes and anti-Stokes detunings as $(\Delta_{as1}, \Delta_{s1}) = (3.9\gamma, -3.9\gamma)$ and $(\Delta_{as2}, \Delta_{s2}) = (3.9\gamma, -3.9\gamma)$ which correspond to maxima of the SFWM efficiency for process A and process B. To get a more complete picture, we also present the numerical results obtained at $\Delta_{as1} = -\Delta_{s1} = 0$ and $\Delta_{as2} = -\Delta_{s2} = 0$ in Fig. 10 and Fig. 11, where the linear absorption and Raman gain are close to zero (see Fig. 3). Although the overall JSAs are correspondingly reduced, the dependence on pump detunings and Rabi frequencies of the spectral indistinguishability of processes A and B remain quite similar.

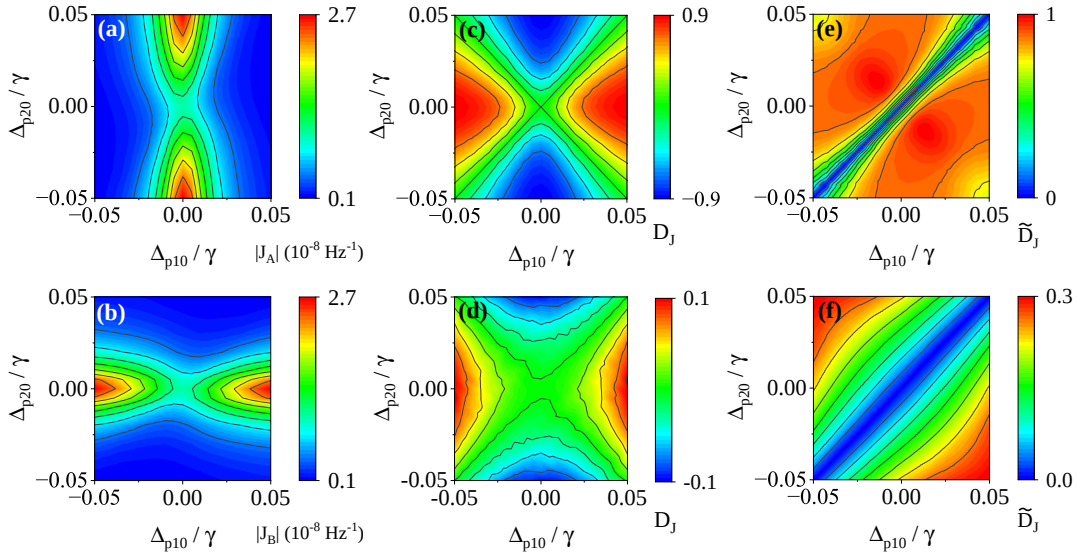

FIG. 10: JSA Moduli $|J_A|$ (a) and $|J_B|$ (b) as well as their normalized mismatch D_J (c, d) and the phase-sensitive metric $\tilde{D}_J$ (e, f) shown for $\Delta_{as1} = -\Delta_{s1} = 0$ and $\Delta_{as2} = -\Delta_{s2} = 0$. All other parameters are the same as in Fig. 6 of the main text.

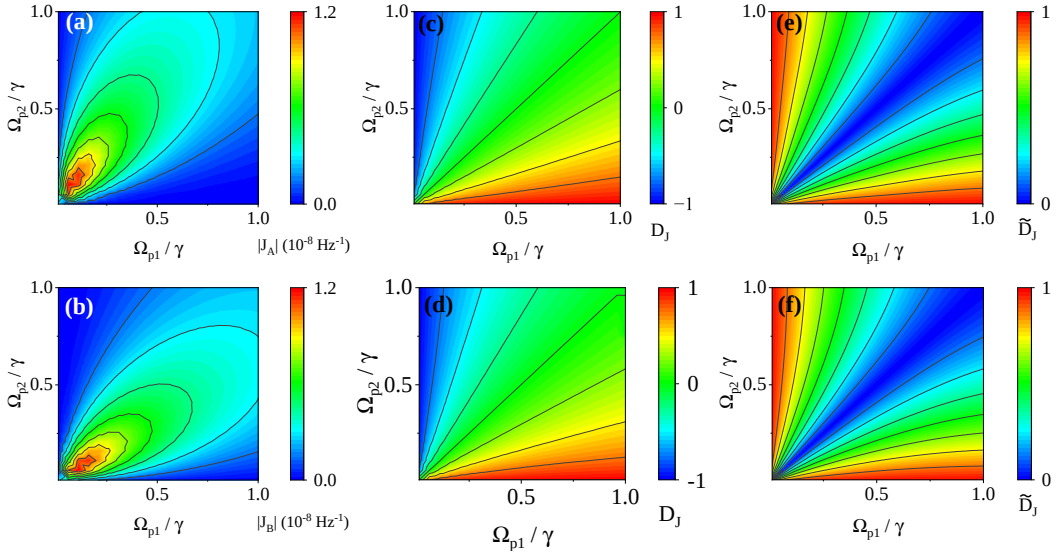

FIG. 11: JSA Moduli $|J_A|$ (a) and $|J_B|$ (b) as well as their normalized mismatch D_J (c, d) and the phase-sensitive metric $\tilde{D}_J$ (e, f) shown for $\Delta_{as1} = -\Delta_{s1} = 0$ and $\Delta_{as2} = -\Delta_{s2} = 0$. All other parameters are the same as in Fig. 8 of the main text.

[1] L. M. Duan, M. D. Lukin, J. I. Cirac and P. Zoller, Long-distance quantum communication with atomic ensembles and linear optics, *Nature (London)* **414**, 413 (2001).

[2] A. MacRae, T. Brannan, R. Achal, and A. I. Lvovsky, Tomography of a High-Purity Narrowband Photon from a Transient Atomic Collective Excitation, *Phys. Rev. Lett.* **109**, 033601 (2012).

[3] J. Roslund, R. M. de Araújo, S. Jiang, C. Fabre, and N. Treps, Wavelength-multiplexed quantum networks with ultrafast frequency combs, *Nat. Photonics* **8**, 109 (2014).

[4] S. Wengerowsky, S. K. Joshi, F. Steinlechner, H. Hübel, and R. Ursin, An entanglement-based wavelength-multiplexed quantum communication network, *Nature (London)* **564**, 225 (2018).

[5] F. Sbresny, L. Hanschke, E. Schöll, W. Rauhaus, B. Scaparra, K. Boos, E. Z. Casalengua, H. Riedl, E. del Valle, J. J. Finley, K. D. Jöns, and K. Müller, Stimulated Generation of Indistinguishable Single Photons from a Quantum Ladder System, *Phys. Rev. Lett.* **128**, 093603 (2022).

[6] S. Slussarenko and G. J. Pryde, Photonic quantum information processing: A concise review, *Appl. Phys. Rev.* **6**, 041303 (2019).

[7] J. M. Lukens, A. Dezfooliyan, C. Langrock, M. M. Fejer, D. E. Leaird, and A. M. Weiner, Orthogonal Spectral Coding of Entangled Photons, *Phys. Rev. Lett.* **112**, 133602 (2014).

[8] J. Nunn, L. J. Wright, C. Söller, L. Zhang, I. A. Walmsley, and B. J. Smith, Large-alphabet time-frequency entangled quantum key distribution by means of time-to-frequency conversion, *Opt. Express* **21**, 15959 (2013).

[9] N. Gisin, G. Ribordy, W. Tittel and H. Zbinden, Quantum cryptography, Rev. Mod. Phys. **74**, 145 (2002).

[10] J. L. O'Brien, Optical quantum computing, *Science* **318**, 1567 (2007).

[11] I. Buluta, S. Ashhab and F. Nori, Natural and artificial atoms for quantum computation, *Rep. Prog. Phys.* **74**, 104401 (2011).

[12] D. Bouwmeester, J. Pan K. Mattle, M. Eibl, H. Weinfurter and A. Zeilinger, Experimental quantum teleportation, *Nature (London)* **390**, 575 (1997).

[13] F. Hoffet, J. Lowinski, L. Heller, A. Padrón-Brito, and H. de Riedmatten, Near-unity indistinguishability of single photons emitted from dissimilar and independent atomic quantum nodes, *PRX Quantum* **5**, 030305 (2024).

[14] K. Zielnicki, K. Garay-Palmett, D. Cruz-Delgado, H. Cruz-Ramirez, M. F. O'Boyle, B. Fang, V. O. Lorenz, A. B. U'Ren, and P. G. Kwiat, Joint spectral characterization of photon-pair sources, *J. Mod. Opt.* **65**, 1141 (2018).

[15] C. Zhang, Y.-F. Huang, B.-H. Liu, C.-F. Li, and G.-C. Guo, Spontaneous parametric down-conversion sources for multiphoton experiments, *Adv. Quantum Technol.* **4**, 2000132 (2021).

[16] G. McCaul, A. F. King, and D. I. Bondar, Optical Indistinguishability via Twinning Fields, *Phys. Rev. Lett.* **127**, 113201 (2021).

[17] A. Padrón-Brito, J. Lowinski, P. Farrera, K. Theophilo, and H. de Riedmatten, Probing the indistinguishability of single photons generated by Rydberg atomic ensembles, *Phys. Rev. Res.* **3**, 033287 (2021).

[18] B. Gaál, M. A. Jacobsen, and L. Vannucci, Near-unity efficiency and photon indistinguishability for the "hourglass" single-photon source using suppression of the background emission, *Appl. Phys. Lett.* **121**, 170501 (2022).

[19] C. F. D. Faurby , L. Carosini, H. Cao, P. I. Sund, L. M. Hansen, F. Giorgino, A. B. Villadsen, S. N. van den Hoven, P. Lodahl, S. Paesani, J. C. Loredo, and P. Walther, Purifying Photon Indistinguishability through Quantum Interference, *Phys. Rev. Lett.* **133**, 033604 (2024).

[20] R. Ghosh and L. Mandel, Observation of Nonclassical Effects in the Interference of Two Photons, *Phys. Rev. Lett.* **59**, 1903 (1987).

[21] L. Mandel, Quantum effects in one-photon and two-photon interference, *Rev. Mod. Phys.* **71**, S274 (1999).

[22] C. Okoth, A. Cavanna, T. Santiago-Cruz, and M. V. Chekhova, Microscale Generation of Entangled Photons without Momentum Conservation, *Phys. Rev. Lett.* **123**, 263602 (2019).

[23] L. Stasi, P. Caspar, T. Brydges, H. Zbinden, F. Bussières, and R. Thew, High-efficiency photon-number-resolving detector for improving heralded single-photon sources, *Quantum Sci. Technol.* **8**, 045006 (2023).

[24] Y. Mei, Y. Zhou, S. Zhang, J. Li, K. Liao, H. Yan, S.-L. Zhu and S. Du, Einstein-Podolsky-Rosen energy-time entanglement of narrow-band biphotons, *Phys. Rev. Lett.* **124**, 010509 (2020).

[25] T.-M. Zhao, Y. S. Ihn and Y.-H. Kim, Direct generation of narrow-band hyperentangled photons, *Phys. Rev. Lett.* **122**, 123607 (2019).

[26] L. Zhu, X. Guo, C. Shu, H. Jeong and S. Du, Bright narrowband biphoton generation from a hot rubidium atomic vapor cell, *Appl. Phys. Lett.* **110**, 161101 (2017).

[27] S. Du, J. Wen, and M. H. Rubin, Narrowband biphoton generation near atomic resonance, *J. Opt. Soc. Am. B* **25**, C98 (2008).

[28] L. Zhao, X. Guo, C. Liu, Y. Sun, M. M. T. Loy and S. Du, Photon pairs with coherence time exceeding 1 μs, *Optica* **1**, 84 (2014).

[29] L. Zhao, Y. Su and S. Du, Narrowband biphoton generation in the group delay regime, *Phys. Rev. A* **93**, 033815 (2016).

[30] C. Shu, P. Chen, T. K. A. Chow, L. Zhu, Y. Xiao, M. M. T. Loy and S. Du, Subnatural-linewidth biphotons from a Doppler-broadened hot atomic vapour cell, *Nat. Commun.* **7**, 12783 (2016).

[31] S. Du, P. Kolchin, C. Belthangady, G. Y. Yin, and S. E. Harris, Subnatural linewidth biphotons with controllable temporal length, *Phys. Rev. Lett.* **100**, 183603 (2008).

[32] H.-M. Zhao, X.-J. Zhang, M. Artoni, G. La Rocca, and J.-H. Wu, Biphoton generation enhanced by nonlocal nonlinearity via Rydberg interactions, *Opt. Lett.* **48**, 5105 (2023).

[33] H.-M. Zhao, X.-J. Zhang, M. Artoni, G. C. La Rocca, and J.-H. Wu, Nonlocal Rydberg enhancement for four-wave-mixing biphoton generation, *Phys. Rev. A* **109**, 043711 (2024).

[34] J.-P. W. MacLean, J. M. Donohue, and K. J. Resch, Direct Characterization of Ultrafast Energy-Time Entangled Photon Pairs, *Phys. Rev. Lett.* **120**, 053601 (2018).

[35] W. P. Grice, A. B. U'Ren, and I. A. Walmsley, Eliminating frequency and space-time correlations in multiphoton

states, *Phys. Rev. A* **64**, 063815 (2001).
[36] F. Graffitti, P. Barrow, M. Proietti, D. Kundys, and A. Fedrizzi, Independent high-purity photons created in domain-engineered crystals, *Optica* **5**, 514 (2018).
[37] V. Ansari, J. Donohue, B. Brecht, and C. Silberhorn, Tailoring nonlinear processes for quantum optics with pulsed temporal-mode encodings, *Optica* **5**, 534 (2018).
[38] H.-M. Zhao, X.-J. Zhang, M. Artoni, G. La Rocca, and J.-H. Wu, Photon-pair generation on resonance via a dark state, *Phys. Rev. A* **106**, 023711 (2022).
[39] I. I. Faruque, G. F. Sinclair, D. Bonneau, T. Ono, C. Silberhorn, M. G. Thompson, and J. G. Rarity, Estimating the Indistinguishability of Heralded Single Photons Using Second-Order Correlation, *Phys. Rev. Appl.* **12**, 054029 (2019).
[40] F. Graffitti, J. Kelly-Massicotte, A. Fedrizzi, and A. M. Branczyk, Design considerations for high-purity heralded single-photon sources, *Phys. Rev. A* **98**, 053811 (2018).
[41] A. Zavatta, M. Artoni and G. La Rocca, Engineering of heralded narrowband color-entangled states, *Phys. Rev. A* **99**, 031802 (2019).
[42] Y.-E. Wong , T. H. Chang, and H. H. Jen, Almost indistinguishable single photons via multiplexing cascaded biphotons with cavity modulation and phase compensation, *Phys. Rev. A* **105** 063706 (2022).
[43] A. M. Brańczyk, T. C. Ralph, W. Helwig, and C. Silberhorn, Optimized generation of heralded Fock states using parametric down-conversion, *New J. Phys.* **12** 063001 (2010).
[44] S. Du, E. Oh, J. Wen, and M. H. Rubin, Four-wave mixing in three-level systems: Interference and entanglement, *Phys. Rev. A* **76**, 013803 (2007).
[45] A. Nevet, A. Hayat, P. Ginzburg, and M. Orenstein, Indistinguishable Photon Pairs from Independent True Chaotic Sources, *Phys. Rev.Lett.* **107**, 253601 (2011).
[46] N. Bruno, A. Martin, T. Guerreiro, B. Sanguinetti, and R. T. Thew, Pulsed source of spectrally uncorrelated and indistinguishable photons at telecom wavelengths, *Opt. Express* **22**, 17246-17253 (2014).
[47] M. Riebe, T. Monz, K. Kim, A. S. Villar, P. Schindler, M. Chwalla, M. Hennrich, and R. Blatt, Deterministic entanglement swapping with an ion-trap quantum computer, *Nat. Phys.* **4**, 839 (2008).
[48] N. Sangouard, C. Simon, H. de Riedmatten, and N. Gisin, Quantum repeaters based on atomic ensembles and linear optics, *Rev. Modern Phys.* **83**, 33 (2011).
[49] F. Flamini, N. Spagnolo, and F. Sciarrino, Photonic quantum information processing: a review, *Rep. Prog. Phys.* **82**, 016001 (2019).
[50] O. Morin, J.-D. Bancal, M. Ho, P. Sekatski, V. D'Auria, N. Gisin, J. Laurat, and N. Sangouard, Witnessing Trustworthy Single-Photon Entanglement with Local Homodyne Measurements, *Phys. Rev. Lett.* **110**, 130401 (2013).
[51] F. Monteiro, V. C. Vivoli, T. Guerreiro, A. Martin, J.-D. Bancal, H. Zbinden, R. T. Thew, and N. Sangouard, Revealing Genuine Optical-Path Entanglement, *Phys. Rev. Lett.* **114**, 170504 (2015).
[52] A. Zavatta, M. D'Angelo, V. Parigi, and M. Bellini, Remote Preparation of Arbitrary Time-Encoded Single-Photon Ebits, *Phys. Rev. Lett.* **96**, 020502 (2006).
[53] S. Ramelow, L. Ratschbacher, A. Fedrizzi, N. K. Langford, and A. Zeilinger, Discrete Tunable Color Entanglement, *Phys. Rev. Lett.* **103**, 253601 (2009).
[54] M. X. Dong, W. Zhang, Z. B. Hou, Y. C. Yu, S. Shi, D. S. Ding, and B. S. Shi, Experimental realization of narrowband four-photon Greenberger-Horne-Zeilinger state in a single cold atomic ensemble, *Opt. Lett.* **42**, 4691 (2017).
[55] G. S. Agarwal, Quantum statistical theory of optical-resonance phenomena in fluctuating laser fields, *Phys. Rev. A* **18**, 1490 (1978).
[56] M. Fleischhauer and M. O. Scully, Quantum sensitivity limits of an optical magnetometer based on atomic phase coherence, *Phys. Rev. A* **49**, 1973 (1994).
[57] J. Gea-Banacloche, Y.-Q. Li, S.-Z. Jin, and M. Xiao, Electromagnetically induced transparency in ladder-type inhomogeneously broadened media: Theory and experiment, *Phys. Rev. A* **51**, 576-584 (1995).
[58] A. Rojas-Santana, G. J. Machado, D. Lopez-Mago, and J. P. Torres, Frequency-correlation requirements on the biphoton wave function in an induced-coherence experiment between separate source, *Phys. Rev. A* **102**, 053711 (2020).
[59] R.-B. Jin, W.-H. Cai, C. Ding, F. Mei, G.-W. Deng, R. Shimizu, and Q. Zhou, Spectrally uncorrelated biphotons generated from "the family of BBO crystal", *Quantum Eng.* **2**, e38 (2020).
[60] P. Boucher, H. Defienne, and S. Gigan, Engineering spatial correlations of entangled photon pairs by pump beam shaping, *Opt. Lett.* **46**, 4200 (2021).
[61] C. Chen, J. E. Heyes, K.-H. Hong, M. Y. Niu, A. E. Lita, T. Gerrits, S. W. Nam, J. H. Shapiro, and F. N. C. Wong, Indistinguishable single-mode photons from spectrally engineered biphotons, *Opt. Express* **27**, 11626 (2019).
[62] T. Landes, M. G. Raymer, M. Allgaier, S. Merkouche, B. J. Smith, and A. H. Marcus, Quantifying the enhancement of two-photon absorption due to spectral-temporal entanglement, *Opt. Express* **29**, 20022 (2021).
[63] P. Boucher, H. Defienne, and S. Gigan, Engineering spatial correlations of entangled photon pairs by pump beam shaping, *Opt. Lett.* **46**, 4200 (2021).
[64] P. Kumar, M. Younesi, S. Saravi, F. Setzpfandt, and T. Pertsch, Group-index-matched frequency conversion in lithium niobate on insulator waveguides, *Front. Photon.* **3**, 951499 (2022).
[65] X. Lai, C. Li, A. Zanders, Y. Mei, and S. Du, Symmetry Protected Two-Photon Coherence Time, Phys. Rev. Lett. **133**, 033601 (2024).
[66] J.-K. Lin, T.-H. Chien, C.-T. Wu, R. Chinnarasu, S. Du, Ite A. Yu, and C.-S. Chuu, Observation of Subnatural-Linewidth Biphotons in a Two-Level Atomic Ensemble, Phys. Rev. Lett. **134**, 043602 (2025).
[67] P. Wan, W.-Z. Zhu, Y.-C. Lou, Z.-M. Cheng, Z.-C. Ren, H. Zhang, X.-L. Wang, and H.-T. Wang, Postselection-Free Cavity-Enhanced Narrow-Band Orbital Angular Momentum Entangled Photon Source, Phys. Rev. Lett. **134**, 053801 (2025).
[68] K. Bergmann, H. Theuer and B. W. Shore, Coherent population transfer among quantum states of atoms and molecules, *Rev. Mod. Phys.* **70**, 1003 (1998).
[69] H. R. Gray, R. M. Whitley and C. R. Stroud, Coherent trapping of atomic populations, *Opt. Lett.* **3**, 218 (1978).
[70] M. Fleischhauer and M. D. Lukin, Dark-state polaritons in electromagnetically induced transparency, *Phys. Rev. Lett.* **84**, 5094 (2000).
[71] J.-H. Wu, C.-L. Cui, N. Ba, Q.-R. Ma and J.-Y. Gao, Dynamical evolution and analytical solutions for multiple

degenerate dark states in the tripod-type atomic system, *Phys. Rev. A* **75**, 043819 (2007).

[72] H.-M. Zhao, D.-D. Zheng, X.-J. Zhang and J.-H. Wu, Broadband tunable transmission non-reciprocity in thermal atoms dominated by two-photon transitions, *New J. Phys.* **26**, 043018 (2024).

[73] Rodney Loudon, *The Quantum Theory of Light* (Oxford Science Publications) 3rd Edition, (2000).

[74] M. Förtsch, J. Fürst, C. Wittmann, D. Strekalov, A. Aiello, M. V. Chekhova, C. Silberhorn, G. Leuchs, and C. Marquardt, A versatile source of single photons for quantum information processing, *Nat. Commun.* **4**, 1818 (2013).

[75] F. Xu, X. Ma, Q. Zhang, H.-K. Lo, and J.-W. Pan, Secure quantum key distribution with realistic devices, *Rev. Mod. Phys.* **92**, 025002 (2020).